Article:
Li, F., Li, K., Peng, C. et al. (2023) Dynamic event-triggered fuzzy non-fragile control of DC microgrids. ISA Transactions, 142. pp. 83-97. ISSN: 0019-0578

https://doi.org/10.1016/j.isatra.2023.07.012

Dynamic event-triggered fuzzy non-fragile control of DC microgrids

Fuqiang Li[a,b,*], Kang Li[b], Chen Peng[c], Lisai Gao[c]

[a] *College of Sciences, Henan Agricultural University, Zhengzhou, 450002, China*
[b] *School of Electronic and Electrical Engineering, University of Leeds, Leeds, LS29JT, UK*
[c] *Shanghai Key Laboratory of Power Station Automation Technology, School of Mechatronics Engineering and Automation, Shanghai University, Shanghai, 200444, China*

Abstract

This paper studies the event-triggered fuzzy non-fragile control of uncertain DC microgrids subject to false data injection (FDI) attacks, controller saturation, network delays and premise mismatching. Firstly, a dynamic event-triggered mechanism (ETM) is proposed, which can save more communication bandwidth than the static ETMs, and remove the complex Zeno-free computation required by the continuous-time ETMs. Secondly, a fuzzy time-delay closed-loop system model is established, which provides a unified framework to study the effects of the dynamic ETM, FDI attacks, uncertainties, saturation, delays and premise mismatching. Thirdly, mean-square exponential stability criteria are established, and co-design method for the saturated fuzzy non-fragile (SFNF) controller and the dynamic ETM is presented. Simulation results confirm that the SFNF controller can stabilize the unstable DC microgrid, while the dynamic ETM significantly reduces the triggering rate by 84.98%. Comparisons show that the proposed controller performs better than the non-fragile controller, fuzzy controller and robust linear controller, and the dynamic ETM achieves a lower triggering rate than the static ETMs.

Keywords: DC microgrids; saturated non-fragile control; T-S fuzzy control; false data injection attacks; dynamic event-triggered mechanism

*Corresponding author. E-mail address: lifuqiang@henau.edu.cn (Fuqiang Li)

1. Introduction

Table 1: Nomenclature.

CPL	constant power load
ESS	energy storage system
TTM	time-triggered mechanism
ETM	event-triggered mechanism
DETM	dynamic event-triggered mechanism
SETM	static event-triggered mechanism
MIET	minimum inter-event time
DoS	denial of service
FDI	false data injection
LKF	Lyapunov-Krasovskii functional
LMIs	linear matrix inequalities
FNF	fuzzy non-fragile
SFNF	saturated fuzzy non-fragile
min	minimum function
col	column matrix
$diag$	diagonal matrix
I	identity matrix
$He\{A\}$	sum of A and A^T, i.e., $A + A^T$
$\mathbb{N}$	natural number set
$\mathbb{R}$	real number set
$\mathbb{E}$	mathematical expectation
$\|\cdot\|$	Euclidean norm
λ_{min}	minimum eigenvalue
$*$	symmetric item in a symmetric matrix

By seamlessly integrating the renewable energy resources into the electric grid, microgrid provides a suite of operational, technical and economic benefits. Compared with the AC microgrid, the DC microgrid has easier interface with energy storage systems and many electric loads due to their natural DC behavior, and issues of harmonics and reactive power are all eliminated [1]. Thus, the DC microgrid has been widely deployed.

In DC microgrids, the tightly regulated power electronic loads often consume constant power, and thus can be seen as constant power loads (CPLs).

However, the CPLs-induced negative impedance decreases the system damping and may even lead to instability. To this end, passive damping methods have been proposed such as adding resistor or capacitor [2], but they are often costly due to physical constraints. As an energy efficient alternative, active damping strategies emulate passive elements such as virtual resistor by modifying converter control loops [3]. However, they can only guarantee small signal stability due to the usage of small signal models [4]. On the other hand, T-S fuzzy model works well in characterizing nonlinear systems [5], and T-S fuzzy control strategy facilitates global stabilization of nonlinear systems based on the linear control theory, which motivates this paper to introduce it into the microgrid control.

For a practical DC microgrid, it is often difficult or even impossible to build the system model, and system parameters often change due to physical degradation and parameter shifting [6]. During controller implementation, inaccuracies and uncertainties often happen due to precision limitation of digital computing, digital-to-analog conversion error and aging. By formulating a DC microgrid as a Lur'e problem with CPLs induced nonlinear terms satisfying quadratic bounds, the work [7] designs a robust linear controller to stabilize the DC microgrid. Although the method [7] brings advantage of low computational complexity, it does not consider system uncertainties. By modeling parameter variations and fluctuations of CPLs current and input voltage as disturbances, the work [8] proposes a H_∞ controller to reject these perturbations. However, the small-signal model based controller [8] may be difficult to implement due to high order polynomials in the denominator. Using the parallel distributed compensation scheme and T-S fuzzy model, the work [9] proposes a fuzzy non-fragile controller, which is resilient to system and controller uncertainties. However, the effect of communication network is ignored. As more distributed DC microgrids are implemented, communication network becomes an important part in control loop. While the communication network brings benefits of high flexibility and low costs, it also poses serious challenges.

One challenge is the constrained network bandwidth. To facilitate the system analysis based on fruitful sampled system theory, most systems adopt periodic control strategy. However, when the system is running at an operating point without disturbances, it is often a waste of network bandwidth to still frequently transmit plant/controller information. To save network bandwidth, an alternative solution to periodic control mode, namely event-triggered control strategy, is proposed, which executes control tasks only

when system needs attention [10]. Due to its distinctive advantage in saving network bandwidth, ETM is attracting more interests. For instance, in [11] the converter only transmits signals to its neighbors when the variation of its controller output surpasses a constant triggering threshold, and the communication burden can be relieved. However, due to the usage of the constant triggering threshold, the triggering rate of the ETM [11] is often high during the transient response. In [12] system states are used to design the triggering threshold, and the multiple energy storage systems in DC microgrids communicate only when the triggering condition is satisfied. Due to the usage of the state-based triggering threshold, the ETM proposed in [12] can achieve a lower triggering rate than the ETM proposed in [11] during the transient response. Using both the system states and a constant to design the triggering threshold, the work [13] presents an event-triggered secondary control strategy for distributed generation units. Although the ETMs proposed in [11, 12, 13] work well in saving network bandwidth, their triggering conditions need to be checked continuously, and thus complex computations are required to exclude Zeno behavior (infinite number of triggering events within a finite time interval [14]). Besides, due to the usage of the fixed triggering parameters, the performances of these ETMs are conservative. Thus, to develop a Zeno-free dynamic ETM for uncertain DC microgrids is another motivation.

Another network-induced challenge is cyber attacks. FDI attacks intend to inject false data into the original data packets, while denial of service (DoS) attacks attempt to block data transmission [15]. Since FDI attacks can often be intentionally designed to bypass the defense systems, they are more stealthy and destructive, which is drawing increasing attentions. For instance, for cooperative DC microgrids subject to the FDI attacks and uncertainties, a sliding-mode observer [16] and adaptive observer [17] are used to reconstruct and mitigate the false data. However, since these works use the linear PI controllers, stability can only be guaranteed in a region of attraction around the equilibrium point. For time-varying FDI attacks, [18] presents an online identification mechanism and an adaptive model predictive controller to mitigate attacks. Although the aforementioned works present useful results under the continuous-time framework, when using the ETM, the results can not be directly used. Besides, when considering the effect of the ETM and network delays, it is difficult for the controller and microgrids to share the same information, which results in the premise mismatching issue. Further, due to physical restrictions, if the value of control signals surpasses

the maximum allowable output of actuators, saturated nonlinearity appears and jeopardizes system performance [19]. Thus, it is necessary to design an FDI-attack-resilient controller for uncertain DC microgrids while considering the effects of the ETM, delays, premise mismatching and saturation.

To address the aforementioned issues, this paper study the event-triggered fuzzy non-fragile control of uncertain DC microgrids subject to the FDI attacks, saturation, delays and premise mismatching. Main contributions are summarized as follows.

- First, for DC microgrids with CPLs, a novel dynamic ETM is proposed, which can save more network bandwidth than the static ETMs [20, 21, 22], and remove the complex Zeno-behavior-related computation required by the continuous-time ETMs [11, 12, 13].
- Second, a fuzzy time-delay closed-loop system model for DC microgrids with CPLs is established, which makes it possible to study the effects of the dynamic ETM, uncertainties, FDI attacks, saturation, network delays and premise mismatching all in one framework.
- Third, mean-square exponential stability criteria for DC microgrids with CPLs are derived, which establish the relationship between system stability and the affecting factors. Co-design conditions for the SFNF controller and the dynamic ETM are derived, which provide a framework to make tradeoffs between communication and control performances.

The paper is organised as follows. Section 2 presents the modeling process of the DC microgrid control system. System stability is analysed in Section 3, and Section 4 provides the co-design conditions for the SFNF controller and the dynamic ETM. Section 5 presents case studies to confirm the proposed method, and conclusion is given in Section 6.

2. Modeling of the DC microgrid

2.1. System description

As shown in Figure 1, a DC microgrid comprises Q CPLs, an energy storage system (ESS) and a DC source. The CPLs refer to the tightly-regulated loads drawing constant power from converters. The ESS is used to inject current, and the DC source maintains the DC bus. Figure 2 shows

the circuit diagram of the DC microgrid. First, the voltage and current states of the DC microgrid are sampled periodically. Then, the dynamic ETM (DETM) determines whether or not to transmit the sampled data. The SFNF controller receives plant states from the dynamic ETM through a communication network. The controller output is randomly manipulated by the FDI attacks.

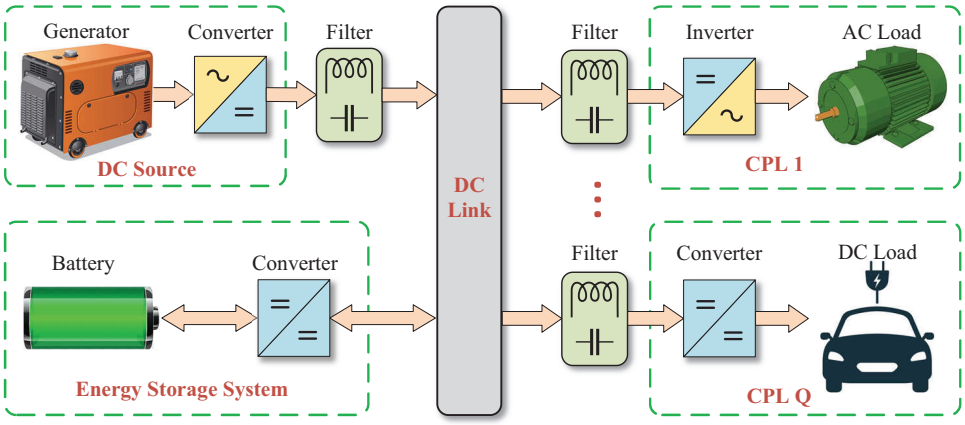

Figure 1: A DC microgrid with Q CPLs.

Applying the Kirchhoff voltage/current laws to the CPL and DC source subsystems yields [7]

$$\cdot\ j_{th} \text{ CPL subsystem: } \begin{cases} \dot{i}_{L,j} = \frac{1}{L_j} v_{C,s} - \frac{1}{L_j} v_{C,j} - \frac{r_{L,j}}{L_j} i_{L,j} \\ \dot{v}_{C,j} = \frac{1}{C_j} i_{L,j} - \frac{1}{C_j} \frac{P_j}{v_{C,j}}, j = 1, \ldots, Q \end{cases} \tag{1}$$

$$\cdot \text{ DC source subsystem: } \begin{cases} \dot{i}_{L,s} = \frac{1}{L_s} V_{dc} - \frac{1}{L_s} v_{C,s} - \frac{r_{L,s}}{L_s} i_{L,s} \\ \dot{v}_{C,s} = \frac{1}{C_s} i_{L,s} - \frac{1}{C_s} \Sigma_{j=1}^{Q} i_{L,j} - \frac{1}{C_s} i_{es} \end{cases} \tag{2}$$

where L_j, C_j and $r_{L,j}$ refer to the inductance, capacitance and resistance in the j_{th} CPL subsystem, respectively. $i_{L,j}$ and $v_{C,j}$ indicate the inductor current and capacitor voltage, respectively. The voltage-controlled current source $P_j/v_{C,j}$ denotes the j_{th} CPL with a constant load power P_j. In the DC source subsystem, L_s, C_s and $r_{L,s}$ indicate the inductance, capacitance and resistance, respectively. $i_{L,s}$ and $v_{C,s}$ refer to the inductor current and capacitor voltage, respectively. V_{dc} denotes the voltage of the DC source, and i_{es} represents the injection current of the ESS.

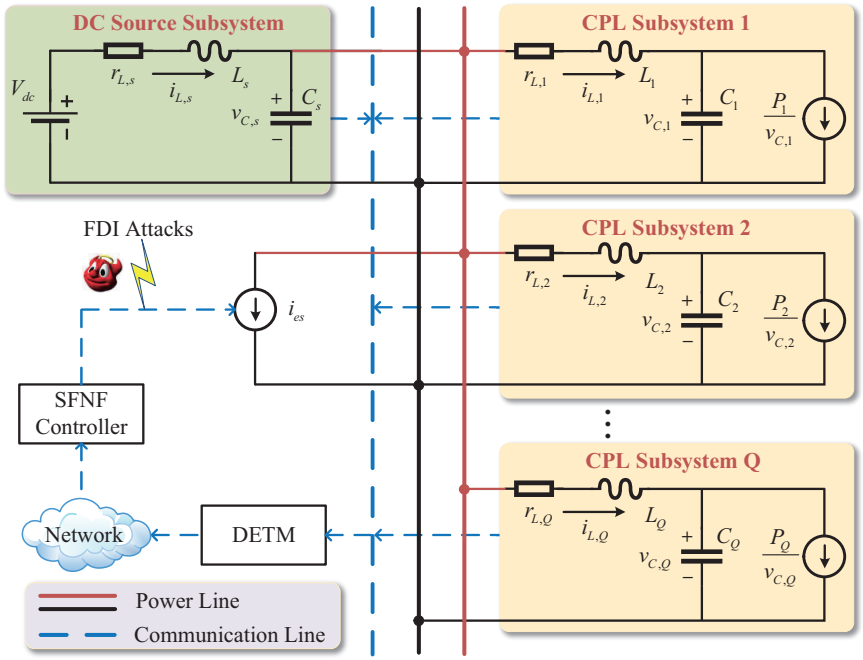

Figure 2: Circuit diagram of the DC microgrid with Q CPLs.

It follows from (1) and (2) that

$$\begin{cases} \dot{x}_j(t) = \bar{A}_j x_j(t) + \bar{A}_{js} x_s(t) - d_j h_j(x_j(t)), j = 1, \ldots, Q \\ \dot{x}_s(t) = \bar{A}_s x_s(t) + \sum_{j=1}^{Q} \bar{A}_{cn} x_j(t) + b_{es} i_{es} + b_s V_{dc} \end{cases} \tag{3}$$

where $x_s(t) = col\{i_{L,s}, v_{C,s}\}$, $x_j(t) = col\{i_{L,j}, v_{C,j}\}$, $h_j(x_j(t)) = \frac{1}{v_{C,j}}$ and

$$\begin{cases} \bar{A}_j = \begin{bmatrix} -\frac{r_{L,j}}{L_j} & -\frac{1}{L_j} \\ \frac{1}{C_j} & 0 \end{bmatrix}, \bar{A}_{js} = \begin{bmatrix} 0 & \frac{1}{L_j} \\ 0 & 0 \end{bmatrix}, d_j = \begin{bmatrix} 0 \\ \frac{P_j}{C_j} \end{bmatrix}, b_s = \begin{bmatrix} \frac{1}{L_s} \\ 0 \end{bmatrix} \\ \bar{A}_s = \begin{bmatrix} -\frac{r_{L,s}}{L_s} & -\frac{1}{L_s} \\ \frac{1}{C_s} & 0 \end{bmatrix}, \bar{A}_{cn} = \begin{bmatrix} 0 & 0 \\ -\frac{1}{C_s} & 0 \end{bmatrix}, b_{es} = \begin{bmatrix} 0 \\ -\frac{1}{C_s} \end{bmatrix} \end{cases}$$

Using (3), the DC microgrid model can be derived as

$$\dot{x}(t) = \bar{A}x(t) + B_{es} i_{es}(t) + B_s V_{dc} - DH(x(t)) \tag{4}$$

where

$x(t) = col\{x_1(t), \ldots, x_Q(t), x_s(t)\}, H(x(t)) = col\{h_1(x_1(t)), \ldots, h_Q(x_Q(t))\}$

$$\bar{A} = \begin{bmatrix} \bar{A}_1 & \ldots & 0 & \bar{A}_{1s} \\ \vdots & \ddots & \vdots & \vdots \\ 0 & \ldots & \bar{A}_Q & \bar{A}_{Qs} \\ \bar{A}_{cn} & \ldots & \bar{A}_{cn} & \bar{A}_s \end{bmatrix}, B_{es} = \begin{bmatrix} 0 \\ \vdots \\ 0 \\ b_{es} \end{bmatrix}, B_s = \begin{bmatrix} 0 \\ \vdots \\ 0 \\ b_s \end{bmatrix}, D = \begin{bmatrix} d_1 & \ldots & 0 \\ \vdots & \ddots & \vdots \\ 0 & \ldots & d_Q \\ 0 & \ldots & 0 \end{bmatrix}$$

To shift the equilibrium point to the origin, using a coordinate transformation to (4) yields

$$\dot{\bar{x}}(t) = \bar{A}\bar{x}(t) + B_{es}\bar{i}_{es}(t) + DH(\bar{x}(t)) \tag{5}$$

where $\bar{x}(t) = col\{\bar{x}_1(t), \ldots, \bar{x}_Q(t), \bar{x}_s(t)\} = x(t) - x_0$, $\bar{x}_j(t) = col\{\bar{i}_{L,j}, \bar{v}_{C,j}\}$, $\bar{x}_s(t) = col\{\bar{i}_{L,s}, \bar{v}_{C,s}\}$, $H(\bar{x}(t)) = col\{h_1(\bar{x}_1(t)), \ldots, h_Q(\bar{x}_Q(t))\}$, and

$$h_j(\bar{x}_j(t)) = \frac{\bar{v}_{C,j}}{v^0_{C,j}(\bar{v}_{C,j} + v^0_{C,j})} \tag{6}$$

where $v^0_{C,j}$ and x_0 indicate the equilibrium points of the voltage $v_{C,j}$ and the DC microgrid, respectively.

2.2. T-S fuzzy modeling of the DC microgrid

Since a microgrid with several CPLs can be modelled as an equivalent system with one CPL [23], without loss of generality, a DC microgrid with one CPL is studied here. If $-\bar{v}^m_{C,1} \leq \bar{v}_{C,1} \leq \bar{v}^m_{C,1}$ holds, the CPLs induced nonlinear term $h_1(\bar{x}_1(t))$ in (6) satisfies [24]

$$\mathscr{K}_{min}\bar{v}_{C,1} \leq h_1(\bar{x}_1(t)) \leq \mathscr{K}_{max}\bar{v}_{C,1} \tag{7}$$

where

$$\mathscr{K}_{min} = \frac{1}{v^0_{C,1}(\bar{v}^m_{C,1} + v^0_{C,1})}, \ \mathscr{K}_{max} = \frac{1}{v^0_{C,1}(-\bar{v}^m_{C,1} + v^0_{C,1})}$$

Using the sector nonlinearity method [25], it follows from (7) that

$$h_1(\bar{x}_1(t)) = \eta_1(\bar{x}_1(t))\mathscr{K}_{min}\bar{v}_{C,1} + \eta_2(\bar{x}_1(t))\mathscr{K}_{max}\bar{v}_{C,1} \tag{8}$$

where membership functions satisfy $\eta_1(\bar{x}_1(t)) + \eta_2(\bar{x}_1(t)) = 1$ with

$$\eta_1(\bar{x}_1(t)) = \frac{\mathscr{K}_{max}\bar{v}_{C,1} - h_1(\bar{x}_1(t))}{(\mathscr{K}_{max} - \mathscr{K}_{min})\bar{v}_{C,1}}, \ \eta_2(\bar{x}_1(t)) = \frac{h_1(\bar{x}_1(t)) - \mathscr{K}_{min}\bar{v}_{C,1}}{(\mathscr{K}_{max} - \mathscr{K}_{min})\bar{v}_{C,1}}$$

Substituting (8) into (5), the T-S fuzzy model of the DC microgrid is obtained as

$$\dot{\bar{x}}(t) = \sum_{i=1}^{2} \eta_i(\bar{x}(t))\{A_i\bar{x}(t) + B_{es}\bar{i}_{es}\} \tag{9}$$

where

$$A_i = \begin{bmatrix} \tilde{A}_i & \bar{A}_{1s} \\ \bar{A}_{cn} & \bar{A}_s \end{bmatrix},\ \tilde{A}_1 = \begin{bmatrix} -\frac{r_{L,1}}{L_1} & -\frac{1}{L_1} \\ \frac{1}{C_1} & \frac{P_1}{C_1}\mathscr{K}_{min} \end{bmatrix},\ \tilde{A}_2 = \begin{bmatrix} -\frac{r_{L,1}}{L_1} & -\frac{1}{L_1} \\ \frac{1}{C_1} & \frac{P_1}{C_1}\mathscr{K}_{max} \end{bmatrix}$$

Remark 1. For the CPLs induced nonlinear term, the work in [7] models it as disturbances introduced to a Lur'e system, and a robust linear controller is then designed. As shown in (9), this paper uses a T-S fuzzy model to characterize the CPLs induced nonlinear term, and a fuzzy non-fragile controller is designed in the following. Since the T-S fuzzy method works well in modeling nonlinear systems, better results can be achieved, which are confirmed in the simulation studies.

Further, considering the plant uncertainty, it follows from (9) that

$$\dot{\bar{x}}(t) = \sum_{i=1}^{2} \eta_i(\bar{x}(t))\{(A_i + \Delta A_i)\bar{x}(t) + B_{es}\bar{i}_{es}\} \tag{10}$$

where $\Delta A_i = \mathscr{D}_i\mathscr{F}_i(t)\mathscr{E}_i$ refers to the plant uncertainty, $\mathscr{D}_i$ and $\mathscr{E}_i$ describe the uncertainty structure, and the uncertain function $\mathscr{F}_i(t)$ satisfies $\mathscr{F}_i^T(t)\mathscr{F}_i(t) \leq I$. $\mathscr{D} = \mathscr{D}_i, \mathscr{E} = \mathscr{E}_i$ and $\mathscr{F}(t) = \mathscr{F}_i(t)$ are assumed here.

2.3. Dynamic event-triggered mechanism

To reduce the unnecessary consumption of network bandwidth, inspired by the work [26], a dynamic ETM is introduced as

$$d_{k+1}h = d_kh + min\{jh|\|\Phi^{\frac{1}{2}}\mathscr{C}_{d_k}\|^2 > [\rho_0 + \rho_d(t)]\|\Phi^{\frac{1}{2}}\bar{x}(d_kh)\|^2\} \tag{11}$$

where $\Phi > 0$ is a weighting matrix, h is the sampling period, $d_kh(k, d_k \in \mathbb{N})$ and $d_{k+1}h$ denote the k_{th} and $(k+1)_{th}$ triggering instants, respectively. $\mathscr{C}_{d_k} = \bar{x}(d_kh) - \bar{x}(d_kh + jh)(j \in \mathbb{N})$ indicates the state error between the state $\bar{x}(d_kh)$ at triggering instant d_kh and the state $\bar{x}(d_kh + jh)$ at sampling instant $d_kh + jh$. $\rho_0 \in [0, 1]$ denotes the static threshold parameter, and $\rho_d(t) = \rho_1$

$(\frac{2}{\pi}arctan(\varrho\|\mathscr{C}_{d_k}\|))$ is the dynamic threshold parameter with $\rho_1 \in [0,1]$ and $\varrho \geq 0$. Unlike the time-triggered mechanism (TTM) which transmits all the sampling data, the dynamic ETM only transmits some of the sampling data which satisfy the triggering condition (11), and thus network bandwidth can be saved.

Remark 2. For the continuous-time ETMs [11, 12, 13], it is essential to ensure a positive minimum inter-event time (MIET). Otherwise, Zeno behavior appears, which makes the implementation of ETMs intractable. However, it is not easy for the continuous-time ETMs to exclude Zeno behavior. For instance, the work [27] shows that the popular ETM $t_{i+1} = min\{t > t_i | \|y(t) - y(t_i)\| > \delta_T \|y(t)\|\}$ exists Zeno behavior, where t_i and t_{i+1} denote the i_{th} and $(i+1)_{th}$ triggering instants, respectively, $y(t)$ and $y(t_i)$ denote measurement outputs at time instant t and triggering instant t_i, respectively, and δ_T is the threshold parameter.

To exclude Zeno behavior, one solution is to continuously evaluate the ETM after a certain time bound. For instance, the work [28] proposes an ETM as $t_{i+1} = min\{t \geq t_i + T_{s,min} | |x(t) - x(t_i)| \geq \delta_T\}$, where $x(t)$ and $x(t_i)$ indicate system states at time instant t and triggering instant t_i, respectively, and the time bound $T_{s,min}$ provides a built-in lower bound on the MIET. Another solution is to periodically check the ETM at sampling instants. For instance, the MIET of the proposed ETM (11) is lower bounded by the sampling period h.

Remark 3. Unlike the static ETMs [20, 21, 22] which only use the fixed triggering threshold parameter ρ_0, the dynamic ETM (11) has an additional dynamic triggering threshold term $\rho_d(t)$, which makes it possible to achieve a lower triggering rate. The dynamic term $\rho_d(t)$ is a function of the state-error term $\|\bar{x}(d_k h) - \bar{x}(d_k h + jh)\|$. During the transient response, the large state-error term results in a large $\rho_d(t)$, and thus the dynamic ETM performs much better than the static ETMs. During the steady response, since the small state-error term leads to a small $\rho_d(t)$, the dynamic ETM also performs slightly better than the static ETMs.

Remark 4. There also exist some other DETMs for multi-area power systems [29, 30], electronic circuit systems [31] and electric vehicles [32]. The triggering threshold parameter $\bar{\rho} = \eta(1 - a\, tanh(e^T(t)e(t) - \theta))$ is used in the DETMs [29, 31], while the threshold parameter $\tilde{\rho} = \sigma_1 + \sigma_2 e^{-\varsigma \|\Phi^{0.5} e(t)\|^2}$ is

adopted in the DETMs [30, 32]. As the state-error term $\|e(t)\|$ increases, both of $\tilde{\rho}$ and $\bar{\rho}$ decrease, but the threshold parameter $\hat{\rho} = \rho_0 + \rho_d(t)$ of the proposed DETM (11) increases. Thus, the DETM (11) can achieve a lower triggering rate during the transient response, while the DETMs [29, 30, 31, 32] can obtain a lower triggering rate during the steady-state response. Namely, the proposed DETM (11) provides a useful alternative for the event-triggered control.

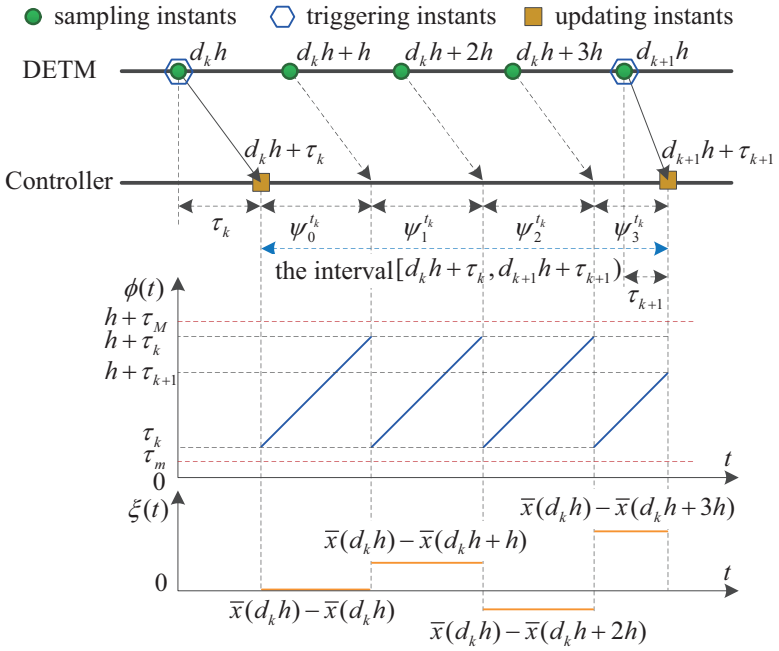

Figure 3: Time sequence of the dynamic ETM.

2.4. Closed-loop system modeling

Considering the effects of the dynamic ETM and network induced delays $\tau_k \in [\tau_m, \tau_M]$, the updating interval of the SFNF controller can be expressed as $[d_k h + \tau_k, d_{k+1} h + \tau_{k+1})$, which can be equally divided as [33] (as illustrated in Figure 3)

$$[d_k h + \tau_k, d_{k+1} h + \tau_{k+1}) = \bigcup_{\epsilon_k = 0}^{\varsigma_k} \psi_{\epsilon_k}^{d_k} \tag{12}$$

where $\varsigma_k = d_{k+1} - d_k - 1$ and

$$\psi_{\epsilon_k}^{d_k} = \begin{cases} [d_k h + \tau_k + \epsilon_k h, d_k h + \tau_k + \epsilon_k h + h), \ \epsilon_k = 0, \ldots, \varsigma_k - 1 \\ [d_k h + \tau_k + \epsilon_k h, d_{k+1} h + \tau_{k+1}), \ \epsilon_k = \varsigma_k \end{cases}$$

During $t \in \psi_{\epsilon_k}^{d_k}$, define a piecewise-constant function $\xi(t) = \bar{x}(d_k h) - \bar{x}(d_k h + \epsilon_k h)$ and a piecewise-linear function $\phi(t) = t - (d_k h + \epsilon_k h) \in [\tau_m, h + \tau_M)$ (as shown in Figure 3). Then, the input signal of the controller can be expressed as

$$\hat{x}(t) = \bar{x}(d_k h) = \xi(t) + \bar{x}(t - \phi(t)), \ t \in \psi_{\epsilon_k}^{d_k} \tag{13}$$

Considering the effects of controller uncertainty and saturation, the SFNF controller can be designed as

$$\hat{\check{i}}_{es} = sat\left\{\check{i}_{es}\right\}, \ \check{i}_{es} = \sum_{j=1}^{2} \bar{\eta}_j(\hat{x}(t))(K_j + \Delta K_j)\hat{x}(t), \ t \in \psi_{\epsilon_k}^{d_k} \tag{14}$$

where

$$\begin{cases} \bar{\eta}_1(\hat{x}(t)) = \frac{\mathscr{K}_{max}\hat{v}_{C,1} - h_1(\hat{x}(t))}{(\mathscr{K}_{max} - \mathscr{K}_{min})\hat{v}_{C,1}}, \bar{\eta}_2(\hat{x}(t)) = 1 - \bar{\eta}_1(\hat{x}(t)) \\ h_1(\hat{x}(t)) = \frac{\hat{v}_{C,1}}{v_{C,1}^0(\hat{v}_{C,1} + v_{C,1}^0)}, \ \ \hat{v}_{C,1} = \bar{v}_{C,1}(d_k h) \end{cases}$$

and $\Delta K_j = \mathscr{D}_j^c \mathscr{U}_j(t) \mathscr{E}_j^c$ marks the controller uncertainty, $\mathscr{D}_j^c$ and $\mathscr{E}_j^c$ indicate the uncertainty structure, and the uncertain function $\mathscr{U}_j(t)$ satisfies ${\mathscr{U}_j}^T(t)\mathscr{U}_j(t) \leq I$. $\mathscr{D}^c = \mathscr{D}_j^c, \mathscr{E}^c = \mathscr{E}_j^c$ and $\mathscr{U}(t) = \mathscr{U}_j(t)$ are assumed here.

Remark 5. As shown in Figure 2, due to the existence of the dynamic ETM and communication network, it is difficult for the controller to share the same premise with the DC microgrid. Unlike the work [23] which assumes the same premise in the controller and plant, the SFNF controller (14) considers the premise mismatching issue, which is more practical.

For an element $\check{i}_{es_j}$ in $\check{i}_{es} \in \mathbb{R}^{n_u} (j = 1, \ldots, n_u)$, the nonlinear saturation function can be described as

$$sat(\check{i}_{es_j}) = \begin{cases} \check{i}_{es_j}^s, & \check{i}_{es_j} > \check{i}_{es_j}^s \\ \check{i}_{es_j}, & -\check{i}_{es_j}^s \leq \check{i}_{es_j} \leq \check{i}_{es_j}^s \\ -\check{i}_{es_j}^s, & \check{i}_{es_j} < -\check{i}_{es_j}^s \end{cases} \tag{15}$$

where $\check{i}^s_{es_j}$ indicates the maximum allowable output threshold, and $\check{i}^s_{es} = \check{i}^s_{es_j}$ is assumed here.

Defining a dead-zone nonlinear function $\mathcal{S}(t) = [\mathcal{S}_1, \mathcal{S}_2, \ldots, \mathcal{S}_{n_u}] = \check{i}_{es} - \hat{i}_{es}$, there exists $\varepsilon_s \in (0,1)$ such that [34]

$$\mathcal{S}(t)^T \mathcal{S}(t) \leq \varepsilon_s \check{i}^T_{es} \check{i}_{es} \tag{16}$$

Remark 6. Similar to [34], using (14), (15) and (16), when $\check{i}_{es_j} > \check{i}^s_{es_j}$, we have $\mathcal{S}_j^2 = [\check{i}_{es_j} - \check{i}^s_{es_j}]^2 \leq \varepsilon^j_s \check{i}^2_{es_j}$, i.e. $\varepsilon^j_s \geq (1 - \check{i}^s_{es_j}/\check{i}_{es_j})^2$, where $\varepsilon^j_s \in (0,1)$. Similarly, when $\check{i}_{es_j} < -\check{i}^s_{es_j}$, $\varepsilon^j_s \geq (1 - \check{i}^s_{es_j}/|\check{i}_{es_j}|)^2$ holds. When $-\check{i}^s_{es_j} \leq \check{i}_{es_j} \leq \check{i}^s_{es_j}$, an arbitrary small ε^j_s satisfies $\mathcal{S}_j^2 = 0 \leq \varepsilon^j_s \check{i}^2_{es_j}$. Considering the above three cases, there exists $\varepsilon^j_s \in (0,1)$ satisfying $\varepsilon^j_s \geq (1 - \check{i}^s_{es_j}/|\check{i}_{es_j}|_{max})^2$, where $|\check{i}_{es_j}|_{max}$ marks the maximum absolute value of $\check{i}_{es_j}$. Setting the maximum value of $\varepsilon^j_s (j = 1, \ldots, n_u)$ as $\varepsilon_s = max\{\varepsilon^j_s\}$, the inequality (16) holds.

Considering the effect of the FDI attacks [35], the SFNF controller (14) is manipulated as

$$\begin{cases} \bar{\check{i}}_{es} = \hat{i}_{es} + \beta(t)\mathscr{A}(t), \ t \in \psi^{d_k}_{\epsilon_k} \\ \hat{i}_{es} = \sum_{j=1}^{2} \bar{\eta}_j(\hat{x}(t))(K_j + \Delta K_j)\hat{x}(t) - \mathcal{S}(t) \end{cases} \tag{17}$$

where $\mathscr{A}(t)$ marks the FDI attack signal, $\beta(t) \in \{0,1\}$ is a Bernoulli distribution with $\mathbb{E}\{\beta(t)\} = \bar{\beta}$. If $\beta(t) = 1$, the attack is active, and thus the controller output is tampered. If $\beta(t) = 0$, the attack is sleeping. To avoid being detected by the defense system, the attacking energy is often limited as $\mathscr{A}^T(t)\mathscr{A}(t) \leq \hat{i}^T_{es} G^T G \hat{i}_{es}$, where G is the upper bound matrix.

Using the DC microgrid model (10) and the attacked SFNF controller (17), the fuzzy time-delay closed-loop system model is obtained as

$$\begin{aligned} \dot{\bar{x}}(t) = \sum_{i=1}^{2}\sum_{j=1}^{2} \eta_i \bar{\eta}_j \big[& (A_i + \Delta A_i)\bar{x}(t) + B_{es}(K_j + \Delta K_j)(\bar{x}(t - \phi(t)) \\ & + \xi(t)) - B_{es}\mathcal{S}(t) + B_{es}\bar{\beta}\mathscr{A}(t) + B_{es}(\beta(t) - \bar{\beta})\mathscr{A}(t) \big] \end{aligned} \tag{18}$$

where $\eta_i = \eta_i(\bar{x}(t))$ and $\bar{\eta}_j = \bar{\eta}_j(\hat{x}(t))$.

Remark 7. Considering the effects of controller uncertainty and saturation, the controller (14) is described as $\hat{i}_{es} = \sum_{j=1}^{2} \bar{\eta}_j(\hat{x}(t)) \, (K_j + \Delta K_j)\hat{x}(t) - \mathcal{S}(t)$. Further, considering the effect of the FDI attacks, the controller (14) is manipulated as $\bar{\check{i}}_{es} = \hat{i}_{es} + \beta(t)\mathscr{A}(t)$ in (17). Substituting the attacked controller (17) into the DC microgrid model (10), the system model (18) is obtained.

3. Stability analysis of the DC microgrid

Definition 1. [36] For any solution $x(t)$ of a system with the initial condition $\mathscr{X}$, the system is exponentially stable in mean square, if there exist $b_1 > 0$ and $b_2 \in [0, 1)$ satisfying

$$\mathbb{E}\{\|x(t)\|^2\} \leq b_1 \|\mathscr{X}\|^2 b_2^t, \ t \geq 0 \tag{19}$$

To simplify the expression, define

$$\begin{cases} \mathscr{I}_i = [\ \overbrace{0\ \ldots\ 0}^{i-1}\ I\ \overbrace{0\ \ldots\ 0}^{7-i}\ ], \quad i = 1, \ldots, 7 \\ \chi(t) = [\bar{x}(t), \bar{x}(t-\phi_1), \bar{x}(t-\phi(t)), \bar{x}(t-\phi_2), \xi(t), \mathscr{A}(t), \mathcal{S}(t)]^T \end{cases} \tag{20}$$

Theorem 1. For given sampling period h, plant and controller uncertainty matrices $\Delta A_i, \Delta K_j$, network delay bounds τ_M, τ_m, dynamic ETM parameters ρ_0, ρ_1, saturation scalar ε_s, attacking expectation $\bar{\beta}$, attack-related matrix G, decay rate μ, and premise-mismatching parameters α_j satisfying $\bar{\eta}_j \geq \alpha_j \eta_j (j = 1, 2)$, if there exist positive definite matrices $P > 0, R > 0, Q > 0, S_1 > 0, S_2 > 0, \Phi > 0$, symmetric matrices Γ^1, Γ^2, and matrix M satisfying $\begin{bmatrix} S_2 & * \\ M & S_2 \end{bmatrix} > 0$ and

$$\Pi^{ij} - \Gamma^i < 0, \ 1 \leq i, j \leq 2 \tag{21}$$

$$\alpha_i(\Pi^{ii} - \Gamma^i) + \Gamma^i < 0, \ i = 1, 2 \tag{22}$$

$$\alpha_j(\Pi^{ij} - \Gamma^i) + \alpha_i(\Pi^{ji} - \Gamma^j) + \Gamma^i + \Gamma^j < 0, \ 1 \leq i < j \leq 2 \tag{23}$$

where

$$\Pi^{ij} = \begin{bmatrix} \Pi_{11}^{ij} & * & * & * \\ \Pi_{21}^{ij} & \Pi_{22} & * & * \\ \Pi_{31} & 0 & \Pi_{33} & * \\ \Pi_{41} & 0 & 0 & \Pi_{44} \end{bmatrix}$$

$\Pi_{11}^{ij} = \Xi^{ij} - {\Psi_1^{ij}}^T(\phi_1^2 S_1 + \phi_{21}^2 S_2)\Psi_1^{ij} - \tilde{\beta}^2 \Psi_2^T(\phi_1^2 S_1 + \phi_{21}^2 S_2)\Psi_2 - \mathscr{I}_5^T \Phi \mathscr{I}_5 - \bar{\beta}\mathscr{I}_6^T \mathscr{I}_6 - \mathscr{I}_7^T \mathscr{I}_7$,

$\Pi_{21}^{ij} = \begin{bmatrix} \phi_1 \Psi_1^{ij} \\ \phi_{21} \Psi_1^{ij} \end{bmatrix}$, $\Pi_{31} = \tilde{\beta} \begin{bmatrix} \phi_1 \Psi_2 \\ \phi_{21} \Psi_2 \end{bmatrix}$, $\Pi_{41} = \begin{bmatrix} \rho^{0.5}(\mathscr{I}_3 + \mathscr{I}_5) \\ G((K_j + \Delta K_j)(\mathscr{I}_3 + \mathscr{I}_5) - \mathscr{I}_7) \\ (K_j + \Delta K_j)(\mathscr{I}_3 + \mathscr{I}_5) \end{bmatrix}$,

$\Pi_{22}=\Pi_{33}=\begin{bmatrix}-S_1^{-1} & * \\ 0 & -S_2^{-1}\end{bmatrix}$, $\Pi_{44}=\begin{bmatrix}-\Phi^{-1} & * & * \\ 0 & -\bar{\beta}^{-1} & * \\ 0 & 0 & -\varepsilon_s^{-1}\end{bmatrix}$,
$\Psi_1^{ij}=(A_i+\Delta A_i)\mathscr{I}_1+B_{es}(K_j+\Delta K_j)(\mathscr{I}_3+\mathscr{I}_5)+\bar{\beta}B_{es}\mathscr{I}_6-B_{es}\mathscr{I}_7$, $\Psi_2=B_{es}\mathscr{I}_6$,
$\Xi^{ij}=\mu\mathscr{I}_1^TP\mathscr{I}_1+He\{\mathscr{I}_1^TP\Psi_1^{ij}\}+\mathscr{I}_1^TR\mathscr{I}_1-e^{-\mu\phi_1}\mathscr{I}_2^TR\mathscr{I}_2+e^{-\mu\phi_1}\mathscr{I}_2^TQ\mathscr{I}_2-e^{-\mu\phi_2}\mathscr{I}_4^TQ\mathscr{I}_4+\Psi_1^{ij^T}(\phi_1^2S_1+\phi_{21}^2S_2)\Psi_1^{ij}+\tilde{\beta}^2\Psi_2^T(\phi_1^2S_1+\phi_{21}^2S_2)\Psi_2-e^{-\mu\phi_1}(\mathscr{I}_1-\mathscr{I}_2)^TS_1(\mathscr{I}_1-\mathscr{I}_2)-e^{-\mu\phi_2}(\mathscr{I}_2-\mathscr{I}_3)^TS_2(\mathscr{I}_2-\mathscr{I}_3)-e^{-\mu\phi_2}(\mathscr{I}_3-\mathscr{I}_4)^TS_2(\mathscr{I}_3-\mathscr{I}_4)-e^{-\mu\phi_2}He\{(\mathscr{I}_3-\mathscr{I}_4)^TM(\mathscr{I}_2-\mathscr{I}_3)\}$, $\tilde{\beta}=(\bar{\beta}(1-\bar{\beta}))^{0.5}$, $\rho=\rho_0+\rho_1$,
then, the DC microgrid system (18) under the dynamic ETM, uncertainties, saturation, FDI attacks, network delays and premise mismatching is exponentially stable in mean square.

Proof. Construct a Lyapunov-Krasovskii functional (LKF) as

$$\begin{aligned}V(t)=&\bar{x}^T(t)P\bar{x}(t)+\phi_1\int_{-\phi_1}^{0}\int_{t+\theta}^{t}e^{\mu(\vartheta-t)}\dot{\bar{x}}^T(\vartheta)S_1\dot{\bar{x}}(\vartheta)d\vartheta d\theta\\&+\int_{t-\phi_2}^{t-\phi_1}e^{\mu(\vartheta-t)}\bar{x}^T(\vartheta)Q\bar{x}(\vartheta)d\vartheta+\int_{t-\phi_1}^{t}e^{\mu(\vartheta-t)}\bar{x}^T(\vartheta)R\bar{x}(\vartheta)d\vartheta\\&+\phi_{21}\int_{-\phi_2}^{-\phi_1}\int_{t+\theta}^{t}e^{\mu(\vartheta-t)}\dot{\bar{x}}^T(\vartheta)S_2\dot{\bar{x}}(\vartheta)d\vartheta d\theta\end{aligned}\tag{24}$$

where positive definite matrices $P>0,R>0,Q>0,S_1>0$ and $S_2>0$, scalars $\phi_1=\tau_m,\phi_2=h+\tau_M$, and $\phi_{21}=\phi_2-\phi_1$.

Computing the derivative of $V(t)$ yields

$$\begin{aligned}\dot{V}(t)\le&-\mu V(t)+\mu\bar{x}^T(t)P\bar{x}(t)+He\{\bar{x}^T(t)P\dot{\bar{x}}(t)\}\\&+e^{-\mu\phi_1}\bar{x}^T(t-\phi_1)Q\bar{x}(t-\phi_1)-e^{-\mu\phi_2}\bar{x}^T(t-\phi_2)Q\bar{x}(t-\phi_2)\\&+\bar{x}^T(t)R\bar{x}(t)-e^{-\mu\phi_1}\bar{x}^T(t-\phi_1)R\bar{x}(t-\phi_1)\\&+\dot{\bar{x}}^T(t)(\phi_1^2S_1+\phi_{21}^2S_2)\dot{\bar{x}}(t)+\delta_1(t)+\delta_2(t)\end{aligned}\tag{25}$$

where

$$\begin{cases}\delta_1(t)=-\phi_1e^{-\mu\phi_1}\int_{t-\phi_1}^{t}\dot{\bar{x}}^T(\theta)S_1\dot{\bar{x}}(\theta)d\theta\\ \delta_2(t)=-\phi_{21}e^{-\mu\phi_2}\int_{t-\phi_2}^{t-\phi_1}\dot{\bar{x}}^T(\theta)S_2\dot{\bar{x}}(\theta)d\theta\end{cases}$$

Using Jensen inequality [37] and applying the reciprocally convex method [38] to $\delta_1(t)$ and $\delta_2(t)$ yields

$$\begin{cases}\delta_1(t)\le-e^{-\mu\phi_1}(\bar{x}(t)-\bar{x}(t-\phi_1))^TS_1(\bar{x}(t)-\bar{x}(t-\phi_1))\\ \delta_2(t)\le-e^{-\mu\phi_2}(\zeta_1^TS_2\zeta_1-\zeta_2^TS_2\zeta_2-He\{\zeta_2^TM\zeta_1\})\end{cases}\tag{26}$$

where $\zeta_1 = [\bar{x}(t-\phi_1) - \bar{x}(t-\phi(t))]$ and $\zeta_2 = [\bar{x}(t-\phi(t)) - \bar{x}(t-\phi_2)]$.

Using (26), it follows from (25) that

$$\mathbb{E}\{\dot{V}(t)\} \leq -\mu\mathbb{E}\{V(t)\} + \sum_{i=1}^{2}\sum_{j=1}^{2} \eta_i\bar{\eta}_j\chi^T(t)\Xi^{ij}\chi(t) \tag{27}$$

Using the triggering, saturation and attacking conditions, it follows from (27) that

$$\begin{aligned}
&\mathbb{E}\{\dot{V}(t)\} + \mu\mathbb{E}\{V(t)\} \\
&\leq \sum_{i=1}^{2}\sum_{j=1}^{2} \eta_i\bar{\eta}_j \big[\chi^T(t)\Xi^{ij}\chi(t) - \xi^T(t)\Phi\xi(t) - \mathcal{S}^T(t)\mathcal{S}(t) \\
&\quad - \bar{\beta}\mathscr{A}^T(t)\mathscr{A}(t) + \rho(\bar{x}(t-\phi(t)) + \xi(t))^T\Phi(\bar{x}(t-\phi(t)) + \xi(t)) \\
&\quad + \varepsilon_s\mathscr{B}^T\mathscr{B} + \bar{\beta}(\mathscr{B} - \mathcal{S}(t))^T G^T G(\mathscr{B} - \mathcal{S}(t)) \\
&\leq \sum_{i=1}^{2}\sum_{j=1}^{2} \eta_i\bar{\eta}_j\chi^T(t)\Pi^{ij}\chi(t)
\end{aligned} \tag{28}$$

where $\mathscr{B} = (K_j + \Delta K_j)(\bar{x}(t-\phi(t)) + \xi(t))$ and
$\Pi^{ij} = \Xi^{ij} - \mathscr{I}_5^T\Phi\mathscr{I}_5 - \bar{\beta}\mathscr{I}_6^T\mathscr{I}_6 - \mathscr{I}_7^T\mathscr{I}_7 + \rho(\mathscr{I}_3 + \mathscr{I}_5)^T\Phi(\mathscr{I}_3 + \mathscr{I}_5) + \varepsilon_s(\mathscr{I}_3 + \mathscr{I}_5)^T(K_j+\Delta K_j)^T(K_j+\Delta K_j)(\mathscr{I}_3+\mathscr{I}_5) + \bar{\beta}((K_j+\Delta K_j)(\mathscr{I}_3+\mathscr{I}_5) - \mathscr{I}_7)^T G^T G((K_j + \Delta K_j)(\mathscr{I}_3 + \mathscr{I}_5) - \mathscr{I}_7)$.

To handle the premise mismatching issue [39], a zero term $\sum_{i=1}^{2}\sum_{j=1}^{2} \eta_i(\eta_j - \bar{\eta}_j)\chi^T(t)\Gamma^i\chi(t) = 0$ is introduced. Adding this zero term to (28) yields

$$\begin{aligned}
&\sum_{i=1}^{2}\sum_{j=1}^{2} \eta_i\bar{\eta}_j\chi^T(t)\Pi^{ij}\chi(t) \\
&= \sum_{i=1}^{2}\sum_{j=1}^{2} \eta_i\bar{\eta}_j\chi^T(t)(\Pi^{ij} - \Gamma^i)\chi(t) + \sum_{i=1}^{2}\sum_{j=1}^{2} \eta_i\eta_j\chi^T(t)\Gamma^i\chi(t)
\end{aligned} \tag{29}$$

Using (21) and $\bar{\eta}_j \geq \alpha_j\eta_j$, if follows from (29) that

$$\begin{aligned}
\sum_{i=1}^{2}\sum_{j=1}^{2} \eta_i\bar{\eta}_j\chi^T(t)\Pi^{ij}\chi(t) &\leq \sum_{i=1}^{2} \eta_i\eta_i\chi^T(t)\left[\alpha_i(\Pi^{ii} - \Gamma^i) + \Gamma^i\right]\chi(t) \\
&+ \sum_{i=1}^{2}\sum_{j>i}^{2} \eta_i\eta_j\chi^T(t)\left[\alpha_j(\Pi^{ij} - \Gamma^i) + \alpha_i(\Pi^{ji} - \Gamma^j) + \Gamma^i + \Gamma^j\right]\chi(t)
\end{aligned} \tag{30}$$

Substituting (22) and (23) into (30) yields $\sum_{i=1}^{2}\sum_{j=1}^{2}\eta_i\bar{\eta}_j\chi^T(t)\Pi^{ij}\chi(t) \leq 0$. Using this inequality, it follows from (28) that

$$\begin{cases} \mathbb{E}\{\dot{V}(t)\} + \mu\mathbb{E}\{V(t)\} \leq 0 \\ \Rightarrow\ \mathbb{E}\{\|\bar{x}(t)\|^2\} \leq \lambda_{\min}^{-1}(P)\mathbb{E}\{V(0)\}e^{-\mu t},\ \forall t \geq 0 \end{cases} \tag{31}$$

Using Definition 1, one can derive from (31) that, the DC microgrid (18) under the dynamic ETM, uncertainties, saturation, FDI attacks, network delays and premise mismatching is exponentially stable in mean square.

Remark 8. For nonlinear systems, it is hard to find a Lyapunov function and design a controller to ensure overall system stability. Using the T-S fuzzy method, this paper models the DC microgrid as a fuzzy binding of a set of linear subsystems, which facilitates using the linear control theory to globally stabilize the nonlinear microgrid [4]. Based on the linear control theory, the LKF (24) and the T-S fuzzy controller (14) are designed. The proposed controller can ensure global stability with simple procedure, which overcomes the limitations that the linear controller only guarantees local stability near the equilibrium point while the design of the nonlinear controller requires a highly complicated procedure [9]. Due to the simple structure, the quadratic Lyapunov functions such as the LKF (24) have been extensively used for stability analysis [40]. As suggested in [41], the non-quadratic Lyapunov functions usually lead to improved convergence and robustness performance, which is an interesting topic in future.

In Theorem 1, gain matrices $K_j (j = 1, 2)$ of the SFNF controller (14) are coupled with the matrices (P, S_1, S_2), which makes the linear matrix inequalities (LMIs) infeasible. Thus, it is necessary to present the following controller design method.

4. Co-design of the SFNF controller and the dynamic ETM

Lemma 1. For a positive definite matrix $\Theta > 0$, a matrix W and any scalar ϵ, the following inequality holds [42]

$$-W\Theta^{-1}W \leq \epsilon^2\Theta - 2\epsilon W \tag{32}$$

Lemma 2. *[43] For a symmetric matrix Λ_1 and matrices Λ_2, Λ_3, if there exists a scalar $\epsilon > 0$ satisfying*

$$\Lambda_1 + \epsilon\Lambda_2\Lambda_2^T + \epsilon^{-1}\Lambda_3^T\Lambda_3 < 0 \tag{33}$$

then, the following inequality holds for all $\mathscr{G}(t)$ satisfying $\mathscr{G}^T(t)\mathscr{G}(t) \leq I$

$$\Lambda_1 + \Lambda_2\mathscr{G}(t)\Lambda_3 + \Lambda_3^T\mathscr{G}^T(t)\Lambda_2^T < 0 \tag{34}$$

Theorem 2. For given sampling period h, uncertainty matrices $\mathscr{D}, \mathscr{E}, \mathscr{D}^c, \mathscr{E}^c$, network delay bounds τ_M, τ_m, dynamic ETM parameters ρ_0, ρ_1, saturation scalar ε_s, attacking expectation $\bar{\beta}$, attack-related matrix G, decay rate μ, scalars $\varepsilon_p, \varepsilon_c, \varepsilon_i > 0 (i = 1, \ldots, 5)$, and premise-mismatching parameters α_j satisfying $\bar{\eta}_j \geq \alpha_j\eta_j (j = 1, 2)$, if there exist positive definite matrices $X > 0, \bar{R} > 0, \bar{Q} > 0, \bar{S}_1 > 0, \bar{S}_2 > 0, \bar{\Phi} > 0$, symmetric matrices $\bar{\Gamma}^1, \bar{\Gamma}^2$, matrices Y_1, Y_2 and M satisfying $\begin{bmatrix} \bar{S}_2 & * \\ \bar{M} & \bar{S}_2 \end{bmatrix} > 0$ and

$$\bar{\Pi}^{ij} - \bar{\Gamma}^i < 0,\ 1 \leq i, j \leq 2 \tag{35}$$

$$\alpha_i(\bar{\Pi}^{ii} - \bar{\Gamma}^i) + \bar{\Gamma}^i < 0,\ i = 1, 2 \tag{36}$$

$$\alpha_j(\bar{\Pi}^{ij} - \bar{\Gamma}^i) + \alpha_i(\bar{\Pi}^{ji} - \bar{\Gamma}^j) + \bar{\Gamma}^i + \bar{\Gamma}^j < 0,\ 1 \leq i < j \leq 2 \tag{37}$$

where

$$\bar{\Pi}^{ij} = \begin{bmatrix} \bar{\Pi}_{11}^{ij} & * & * & * & * & * & * & * \\ \bar{\Pi}_{21}^{ij} & \bar{\Pi}_{22} & * & * & * & * & * & * \\ \bar{\Pi}_{31} & 0 & \bar{\Pi}_{33} & * & * & * & * & * \\ \bar{\Pi}_{41} & 0 & 0 & \bar{\Pi}_{44} & * & * & * & * \\ \bar{\Pi}_{51} & \bar{\Pi}_{52} & 0 & 0 & \bar{\Pi}_{55} & * & * & * \\ \bar{\Pi}_{61} & 0 & 0 & 0 & 0 & \bar{\Pi}_{66} & * & * \\ \bar{\Pi}_{71} & \bar{\Pi}_{72} & 0 & \bar{\Pi}_{74} & 0 & 0 & \bar{\Pi}_{77} & * \\ \bar{\Pi}_{81} & 0 & 0 & 0 & 0 & 0 & 0 & \bar{\Pi}_{88} \end{bmatrix}$$

$\bar{\Pi}_{11}^{ij} = \mu\mathscr{I}_1^T X\mathscr{I}_1 + He\{\mathscr{I}_1^T\bar{\Psi}_1^{ij}\} + \mathscr{I}_1^T\bar{R}\mathscr{I}_1 - e^{-\mu\phi_1}\mathscr{I}_2^T\bar{R}\mathscr{I}_2 + e^{-\mu\phi_1}\mathscr{I}_2^T\bar{Q}\mathscr{I}_2 - e^{-\mu\phi_2}\mathscr{I}_4^T\bar{Q}\mathscr{I}_4 - e^{-\mu\phi_1}(\mathscr{I}_1 - \mathscr{I}_2)^T\bar{S}_1(\mathscr{I}_1 - \mathscr{I}_2) - e^{-\mu\phi_2}(\mathscr{I}_2 - \mathscr{I}_3)^T\bar{S}_2(\mathscr{I}_2 - \mathscr{I}_3) - e^{-\mu\phi_2}(\mathscr{I}_3 - \mathscr{I}_4)^T\bar{S}_2(\mathscr{I}_3 - \mathscr{I}_4) - e^{-\mu\phi_2}He\{(\mathscr{I}_3 - \mathscr{I}_4)^T\bar{M}(\mathscr{I}_2 - \mathscr{I}_3)\} - \mathscr{I}_5^T\bar{\Phi}\mathscr{I}_5 - \bar{\beta}\mathscr{I}_6^T\mathscr{I}_6 - \mathscr{I}_7^T\mathscr{I}_7,$

$\bar{\Pi}_{21}^{ij} = \begin{bmatrix} \phi_1 \bar{\Psi}_1^{ij} \\ \phi_{21} \bar{\Psi}_1^{ij} \end{bmatrix}$, $\bar{\Pi}_{22} = \begin{bmatrix} \varepsilon_1^2 \bar{S}_1 - 2\varepsilon_1 X & * \\ 0 & \varepsilon_2^2 \bar{S}_2 - 2\varepsilon_2 X \end{bmatrix}$,
$\bar{\Pi}_{31} = \tilde{\beta} \begin{bmatrix} \phi_1 \bar{\Psi}_2 \\ \phi_{21} \bar{\Psi}_2 \end{bmatrix}$, $\bar{\Pi}_{33} = \begin{bmatrix} \varepsilon_3^2 \bar{S}_1 - 2\varepsilon_3 X & * \\ 0 & \varepsilon_4^2 \bar{S}_2 - 2\varepsilon_4 X \end{bmatrix}$,
$\bar{\Pi}_{41} = \begin{bmatrix} \rho^{0.5} X(\mathscr{I}_3 + \mathscr{I}_5) \\ G(Y_j(\mathscr{I}_3 + \mathscr{I}_5) - \mathscr{I}_7) \\ Y_j(\mathscr{I}_3 + \mathscr{I}_5) \end{bmatrix}$, $\bar{\Pi}_{44} = \begin{bmatrix} \varepsilon_5^2 \bar{\Phi} - 2\varepsilon_5 X & * & * \\ 0 & -\bar{\beta}^{-1} & * \\ 0 & 0 & -\varepsilon_s^{-1} \end{bmatrix}$,
$\bar{\Pi}_{51} = \varepsilon_p \mathscr{D}^T \mathscr{I}_1, \bar{\Pi}_{52} = \varepsilon_p [\phi_1 \mathscr{D}^T \ \phi_{21} \mathscr{D}^T]$, $\bar{\Pi}_{61} = \mathscr{E} X \mathscr{I}_1$, $\bar{\Pi}_{55} = \bar{\Pi}_{66} = -\varepsilon_p$,
$\bar{\Pi}_{71} = \varepsilon_c \mathscr{D}^{cT} B^T \mathscr{I}_1$, $\bar{\Pi}_{72} = \varepsilon_c [\phi_1 \mathscr{D}^{cT} B^T \ \phi_{21} \mathscr{D}^{cT} B^T]$, $\bar{\Pi}_{74} = \varepsilon_c [0 \ G^T \ I]$,
$\bar{\Pi}_{81} = \mathscr{E}^c X(\mathscr{I}_3 + \mathscr{I}_5)$, $\bar{\Pi}_{77} = \bar{\Pi}_{88} = -\varepsilon_c$, $\tilde{\beta} = (\bar{\beta}(1-\bar{\beta}))^{0.5}$, $\rho = \rho_0 + \rho_1$,
$\bar{\Psi}_1^{ij} = A_i X \mathscr{I}_1 + B_{es} Y_j (\mathscr{I}_3 + \mathscr{I}_5) + \bar{\beta} B_{es} \mathscr{I}_6 - B_{es} \mathscr{I}_7, \bar{\Psi}_2 = B_{es} \mathscr{I}_6$,
$\bar{\Gamma}^i = \Upsilon \Gamma^i \Upsilon (i = 1, 2)$, $\bar{R} = XRX, \bar{Q} = XQX, \bar{S}_1 = XS_1X, \bar{S}_2 = XS_2X, \bar{M} = XMX, \bar{\Phi} = X\Phi X, Y_j = K_j X (j = 1, 2)$,
then, the DC microgrid (18) under the dynamic ETM, FDI attacks, uncertainties, saturation, network delays and premise mismatching is exponentially stable in mean square, and gain matrices of the SFNF controller (14) can be obtained as $K_j = Y_j X^{-1}$.

PROOF. To decouple the nonlinear terms in Theorem 1, define

$$X = P^{-1}, \ \Upsilon = diag\{\underbrace{X, \ldots, X}_{5}, \underbrace{I, \ldots, I}_{9}\} \tag{38}$$

Using (38), transform the conditions in Theorem 1 as

$$\begin{bmatrix} \bar{S}_2 & * \\ \bar{M} & \bar{S}_2 \end{bmatrix} = diag\{X, X\} \begin{bmatrix} S_2 & * \\ M & S_2 \end{bmatrix} diag\{X, X\} > 0 \tag{39}$$

$$\check{\Pi}^{ij} - \bar{\Gamma}^i = \Upsilon(\Pi^{ij} - \Gamma^i)\Upsilon < 0, \ 1 \le i, j \le 2 \tag{40}$$

$$\alpha_i(\check{\Pi}^{ii} - \bar{\Gamma}^i) + \bar{\Gamma}^i = \Upsilon(\alpha_i(\Pi^{ii} - \Gamma^i) + \Gamma^i)\Upsilon < 0, \ i = 1, 2 \tag{41}$$

$$\begin{aligned} &\alpha_j(\check{\Pi}^{ij} - \bar{\Gamma}^i) + \alpha_i(\check{\Pi}^{ji} - \bar{\Gamma}^j) + \bar{\Gamma}^i + \bar{\Gamma}^j \\ &= \Upsilon(\alpha_j(\Pi^{ij} - \Gamma^i) + \alpha_i(\Pi^{ji} - \Gamma^j) + \Gamma^i + \Gamma^j)\Upsilon < 0, 1 \le i < j \le 2 \end{aligned} \tag{42}$$

where

$$\begin{cases} \check{\Pi}^{ij} = \tilde{\Pi}^{ij} + He\{L_{p1}^T \mathscr{F}_i(t) L_{p2} + L_{c1}^T \mathscr{U}_j(t) L_{c2}\} \\ \tilde{\Pi}^{ij} = \begin{bmatrix} \bar{\Pi}_{11}^{ij} & * & * & * \\ \bar{\Pi}_{21}^{ij} & \Pi_{22} & * & * \\ \bar{\Pi}_{31} & 0 & \Pi_{33} & * \\ \bar{\Pi}_{41} & 0 & 0 & \Pi_{44} \end{bmatrix} \end{cases}$$

with

$$\begin{cases} L_{p1} = [\mathscr{D}^T\mathscr{I}_1 \ \phi_1\mathscr{D}^T \ \phi_{21}\mathscr{D}^T \ 0\ 0\ 0\ 0\ 0] \\ L_{p2} = [\mathscr{E}X\mathscr{I}_1 \ 0\ 0\ 0\ 0\ 0\ 0\ 0] \\ L_{c1} = [\mathscr{D}^{cT}B^T\mathscr{I}_1 \ \ \phi_1\mathscr{D}^{cT}B^T \ \ \phi_{21}\mathscr{D}^{cT}B^T \ 0\ 0\ 0 \ G^T \ I \ 0\ 0] \\ L_{c2} = [\mathscr{E}^cX(\mathscr{I}_3 + \mathscr{I}_5) \ 0\ 0\ 0\ 0\ 0\ 0\ 0\ 0\ 0] \end{cases}$$

The inequality (40) can be rewritten as

$$\check{\Pi}^{ij} - \bar{\Gamma}^i = \tilde{\Pi}^{ij} - \bar{\Gamma}^i + He\{L_{p1}^T\mathscr{F}_i(t)L_{p2} + L_{c1}^T\mathscr{U}_j(t)L_{c2}\} < 0 \tag{43}$$

Using Lemma 2, (43) holds if the following inequality is satisfied

$$\tilde{\Pi}^{ij} - \bar{\Gamma}^i + \varepsilon_p L_{p1}^T L_{p1} + \varepsilon_p^{-1} L_{p2}^T L_{p2} + \varepsilon_c L_{c1}^T L_{c1} + \varepsilon_c^{-1} L_{c2}^T L_{c2} < 0 \tag{44}$$

Using Schur complement to (44), and then using Lemma 1 to handle the nonlinear terms Π_{22}, Π_{33} and Π_{44} in $\tilde{\Pi}^{ij}$, (35) can be obtained. Similarly, (36) and (37) can be derived. The proof is thus completed.

Remark 9. By computing the LMIs in Theorem 2, gain matrices $K_j = Y_jX^{-1}(j = 1, 2)$ of the SFNF controller (14) and parameter $\Phi = X^{-1}\bar{\Phi}X^{-1}$ of the dynamic ETM (11) can be obtained simultaneously, which is more convenient that the two-step emulation method [44].

5. Case studies

5.1. DC microgrid with one CPL

The DC microgrid in [23] is introduced to verify the proposed method. The microgrid parameters and system parameters are shown in Table 2 and Table 3, respectively.

Table 2: DC microgrid with one CPL.

$r_{L,1}$	1.1 Ω	$v_{C,1}^0$	196.64 V	C_s	500 μF
L_1	39.5 mH	$\bar{v}_{C,1}^m$	130.4 V	V_{dc}	200 V
C_1	500 μF	$r_{L,s}$	1.1 Ω		
P_1	300 W	L_s	39.5mH		

Table 3: System parameters.

dynamic ETM	$\rho_0 = 0.0004, \rho_1 = 0.0006, \varrho = 50$
FDI attacks	$\mathscr{A}(t) = -tanh(G\hat{i}_{es})$, $G = 0.3$, $\bar{\beta} = 0.15$
plant uncertainty	$\Delta A = sin(t)\begin{bmatrix} -2.2 & -2 & 0 & 2; \\ 0 & 0 & 0 & 0; \\ 0 & 0 & -2.2 & -2; \\ 0 & 0 & 0 & 0 \end{bmatrix}$
controller uncertainty	$\Delta K = 0.1sin(t)\begin{bmatrix} 1 & 1 & 1 & 1 \end{bmatrix}$
controller saturation	$\check{i}^s_{es} = 50A$, $\varepsilon_s = 0.6$
sampling period	$h = 0.05ms$
network-delay bounds	$\tau_M = 0.02ms, \tau_m = 0.01ms$
premise mismatching	$\alpha_1 = 0.9, \alpha_2 = 0.8$
decay rate	$\mu = 10$
Lemma scalars	$\varepsilon_i = 0.000015 (i = 1, \ldots, 5)$, $\varepsilon_p = 100$, $\varepsilon_c = 0.1$
initial states	$\bar{x}_0 = col\{19, -30, 19, -30\}$

Remark 10. In Theorem 2, Lemma 1 is used to transform the nonlinear terms $-X\bar{S}_1^{-1}X$, $-X\bar{S}_2^{-1}X$ and $-X\bar{\Phi}^{-1}X$ into the linear terms $\varepsilon_i^2\bar{S}_1 - 2\varepsilon_i X$ $(i = 1, 3)$, $\varepsilon_i^2\bar{S}_2 - 2\varepsilon_i X (i = 2, 4)$ and $\varepsilon_5^2\bar{\Phi} - 2\varepsilon_5 X$, which makes the LMIs feasible. Since the inequality $-W\Theta^{-1}W \leq \epsilon^2\Theta - 2\epsilon W$ in Lemma 1 holds for any scalar ϵ, the values of the scalars $\varepsilon_i = 0.000015 (i = 1, \ldots, 5)$ in Table 3 are reasonable.

By computing the LMIs in Theorem 2, gain matrices of the SFNF controller and parameter of the dynamic ETM are obtained simultaneously as

$$\begin{cases} K_1 = \begin{bmatrix} 10.8143 & 1.0999 & -0.6837 & 1.6047 \end{bmatrix} \\ K_2 = \begin{bmatrix} 10.7676 & 1.0987 & -0.6865 & 1.5967 \end{bmatrix} \\ \Phi = 10^3 \times \begin{bmatrix} 3.9605 & 0.2922 & -0.1873 & 0.2022 \\ 0.2922 & 0.0844 & -0.1962 & 0.0235 \\ -0.1873 & -0.1962 & 1.5221 & -0.0505 \\ 0.2022 & 0.0235 & -0.0505 & 0.0278 \end{bmatrix} \end{cases} \tag{45}$$

Remark 11. In Theorem 2, due to $K_j = Y_j X^{-1} (j = 1, 2)$, gain matrices K_j of the controller (14) can be adjusted by Y_j and X. If choosing different

system parameters, the LMIs in Theorem 2 can generate different controller gains K_j. For instance, as shown in Table 4, a positive $\Delta\rho = 0.5 \times 10^{-3}$ results in positive $\Delta\|K_1\| = 1.7743$ and $\Delta\|K_2\| = 1.7543$, where $\Delta\rho$ and $\Delta\|K_j\|(j = 1, 2)$ denote the variations of $\rho = \rho_0 + \rho_1$ in Table 3 and $\|K_j\|$ in (45), respectively. Namely, when the triggering threshold increases, the dynamic ETM transmits less data to update the controller, and thus larger controller gains are generated. Similarly, a larger attacking expectation (i.e., $\Delta\bar{\beta} > 0$), a stronger uncertainty (i.e., $\Delta\mathscr{D} > 0$) or more serious saturation (i.e., $\Delta\epsilon_s > 0$) has a more significant negative effect on system performance, where $\Delta\bar{\beta}$, $\Delta\mathscr{D}$ and $\Delta\epsilon_s$ denote the variations of $\bar{\beta}$, $\mathscr{D}$ and ϵ_s, respectively, and thus larger controller gains (i.e., $\Delta\|K_j\| > 0$) are generated. On the other hand, since $\Delta\rho < 0$, $\Delta\bar{\beta} < 0$, $\Delta\mathscr{D} < 0$ or $\Delta\epsilon_s < 0$ implies less negative effect on system performance, smaller controller gains (i.e., $\Delta\|K_j\| < 0$) are produced.

Table 4: Effect of system parameters on the controller

	$\Delta\rho(\times 10^{-3})$		$\Delta\bar{\beta}$		$\Delta\mathscr{D}$		$\Delta\epsilon_s$	
	-0.5	0.5	-0.05	0.05	-0.5	0.5	-0.05	0.05
$\Delta\|K_1\|$	-1.5793	1.7743	-0.5734	0.6056	-0.3424	0.6722	-0.4757	0.5780
$\Delta\|K_2\|$	-1.5693	1.7543	-0.5697	0.5941	-0.3316	0.6499	-0.4873	0.5910

Figure 4 shows the voltage and current responses of the DC microgrid subject to the dynamic ETM, uncertainties, saturation, FDI attacks, delays and premise mismatching. Although the open-loop system is unstable, the proposed SFNF controller works well in stabilizing the DC microgrid. As shown in the data tips, the capacitor voltage $v_{C,1}$ arrivals at its equilibrium point $v^0_{C,1} = 196.64V$, while the inductor current $i_{L,1}$ also reaches its operating point $i^0_{L,1} = P_1/v^0_{C,1} = 1.5256A$.

As shown in Figure 5, the required injection current becomes smaller when system approaches the equilibrium point. As shown in the zoomed graphs, the original injection current is affected by the controller uncertainty. Due to the effect of the saturation, the large current during the time interval $[0, 0.75ms]$ is set to the saturation threshold $50A$. Further, the saturated current is tampered by the FDI attacks. Besides, due to the effect of the dynamic ETM, the injection current holds during each triggering interval.

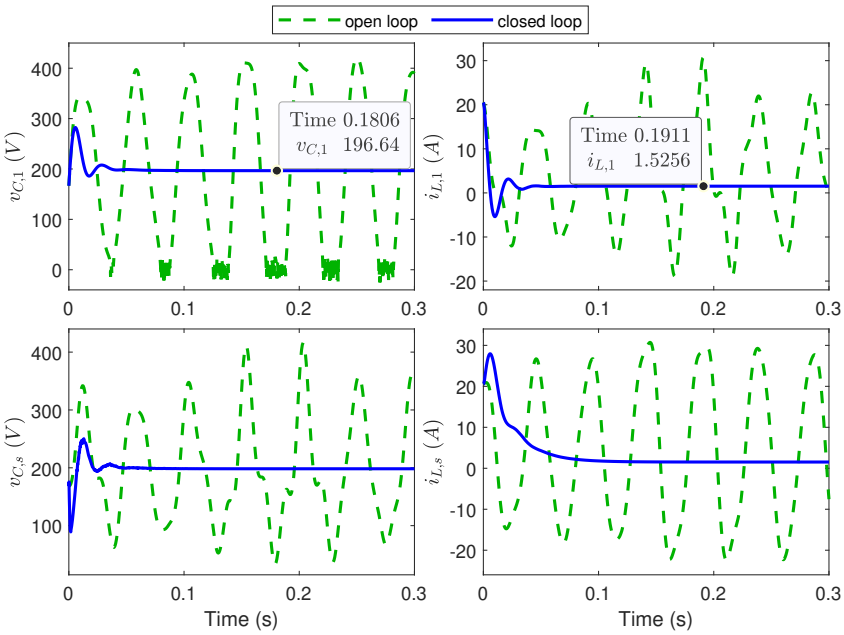

Figure 4: Voltage and current responses of the DC microgrid.

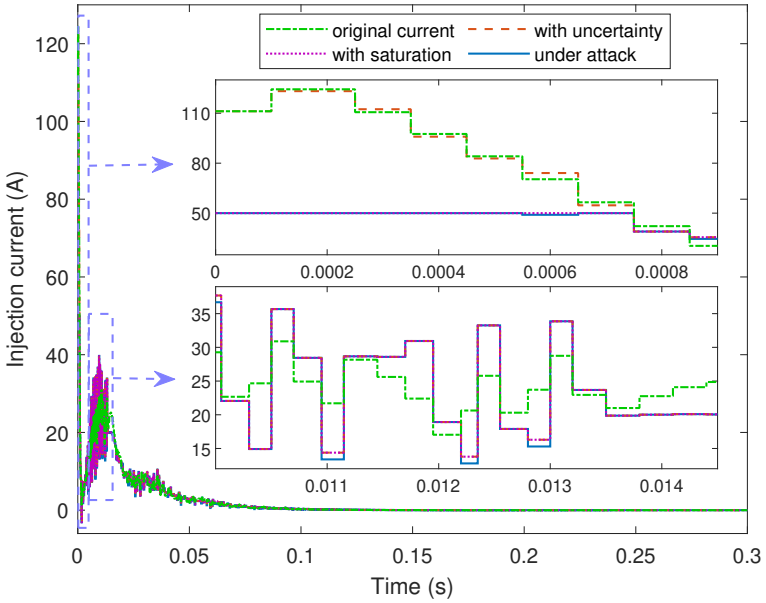

Figure 5: The injection current.

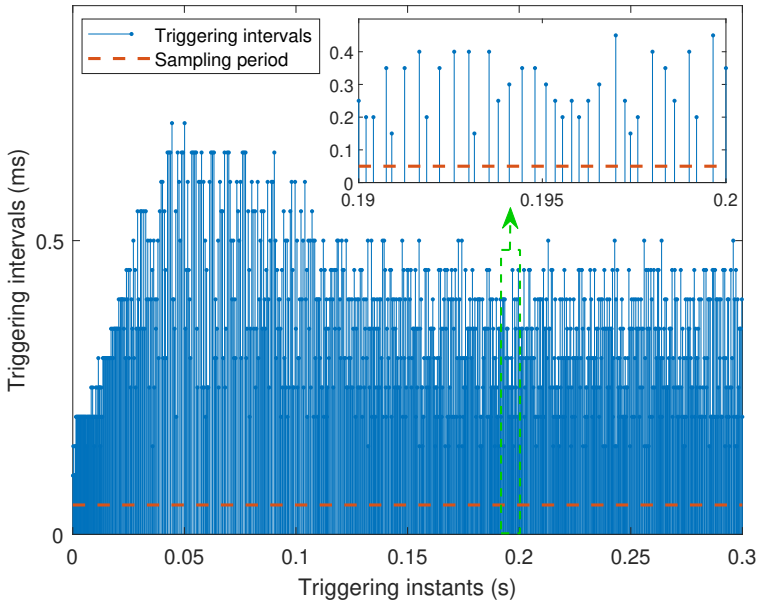

Figure 6: Triggering instants and triggering intervals of the dynamic ETM.

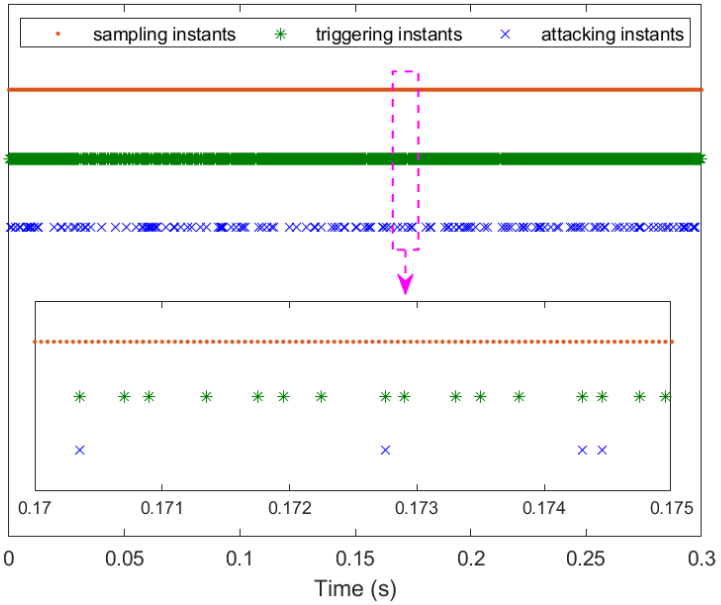

Figure 7: Triggering instants, attacking instants and sampling instants.

Figure 6 shows the triggering instants and triggering intervals of the dynamic ETM. The maximum and average triggering intervals are $0.7ms$ and $0.33ms$, respectively, which are much larger than the sampling period $0.05ms$. The minimum triggering interval is $0.1ms$, which avoids Zeno behavior. Among the 6000 sampling data, only 901 of them are transmitted. Thus, the triggering rate of the dynamic ETM is computed as $R_t = 15.02\%$, which implies 84.98% of communication resources can be saved.

Figure 7 shows the relationship of attacking instants of the FDI attacks, triggering instants of the dynamic ETM and sampling instants. During the time interval $[0, 0.3s]$, among the 901 triggering instants of the dynamic ETM, 157 of them are attacked by the FDI attacks, and thus the attacking rate is computed as $R_a = 17.43\%$.

In summary, for the unstable DC microgrid affected by many factors, the proposed SFNF injection current controller achieves satisfactory control performance, while the dynamic ETM effectively saves communication resources, which confirm effectiveness of the proposed method.

5.2. Comparison with the non-fragile controller [9]

Using the microgrid parameters in [9], Theorem 2 computes the SFNF controller as

$$\begin{cases} K_1 = \begin{bmatrix} 0.3911 & 0.1395 & 1.2506 & 1.1086 \end{bmatrix} \\ K_2 = \begin{bmatrix} 0.4006 & 0.1403 & 1.2318 & 1.1020 \end{bmatrix} \end{cases} \tag{46}$$

Using the non-fragile controller in [9] (i.e., $K_1 = [31.8678\ 62.1220\ 27.2029\ 220.2515]$, $K_2 = [31.8678\ 62.8396\ 27.2029\ 20.2515]$) and the SFNF controller (46), voltage and current responses of the DC microgrid with initial states $\bar{x}_0 = col\{0, 15, 0, 10\}$ are shown in Figure 8. The non-fragile controller [9] can not stabilize the system, since the effects of the FDI attacks, network delays and premise mismatching are not considered when designing the controller. On the other hand, since Theorem 2 considers all the affecting factors, the SFNF controller (46) works well in stabilizing the microgrid.

Besides, the gain norm of the non-fragile controller [9] (i.e., $\|K_1\| = 232.6487, \|K_2\| = 78.1952$) are much larger than that of the SFNF controller (46) (i.e., $\|K_1\| = 1.7220, \|K_2\| = 1.7064$). Since the controller's gain norm corresponds to the energy supplied by the ESS, the SFNF controller (46)

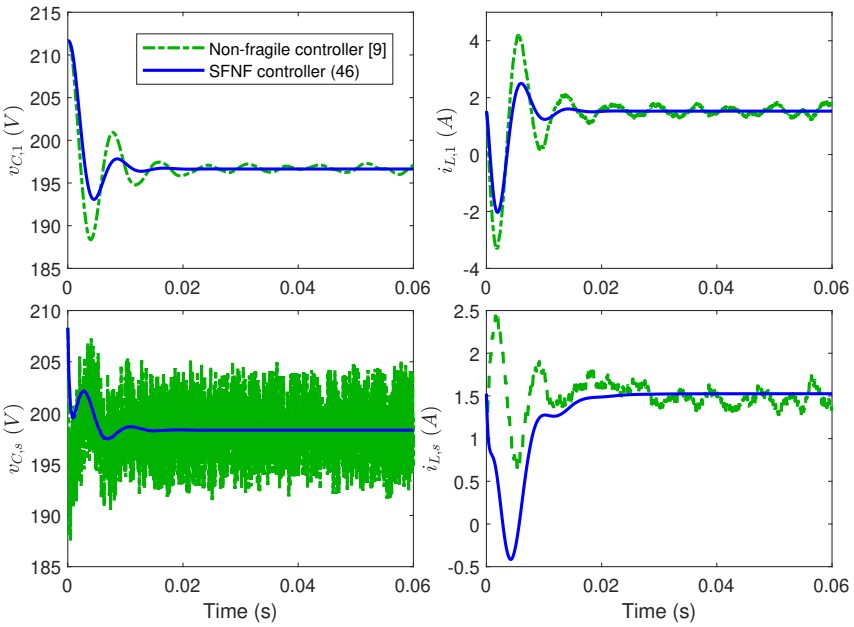

Figure 8: State responses under the non-fragile controller [9] and SFNF controller (46).

consumes less energy than the non-fragile controller [9]. Moreover, the updating frequency of the event-triggered SFNF controller (46) (i.e., the triggering rate 56.25% of the dynamic ETM) is much lower than that of the time-triggered no-fragile controller [9] (i.e., 100%). Thus, the power loss of the SFNF controller (46) is lower than that of the no-fragile controller [9].

5.3. Comparison with different controllers [7, 25]

For the DC microgrid in Section 5.1 only affected by the uncertainties, using the methods in [7, 25] and Theorem 2, the robust linear controller [7], the fuzzy controller [25] and the proposed fuzzy non-fragile (FNF) controller are obtained as follows.

$$\text{Robust linear controller: } K = \begin{bmatrix} -1.0549 & -0.1585 & 0.9932 & 0.1958 \end{bmatrix}$$

$$\text{Fuzzy controller: } \begin{cases} K_1 = \begin{bmatrix} 0.8581 & 0.0420 & 0.8502 & 0.1751 \end{bmatrix} \\ K_2 = \begin{bmatrix} 0.8562 & 0.0428 & 0.8508 & 0.1751 \end{bmatrix} \end{cases}$$

FNF controller:
$$\begin{cases} K_1 = \begin{bmatrix} 47.1117 & 7.0906 & -22.7814 & 2.5468 \end{bmatrix} \\ K_2 = \begin{bmatrix} 43.8730 & 6.9902 & -22.6965 & 2.5287 \end{bmatrix} \end{cases}$$

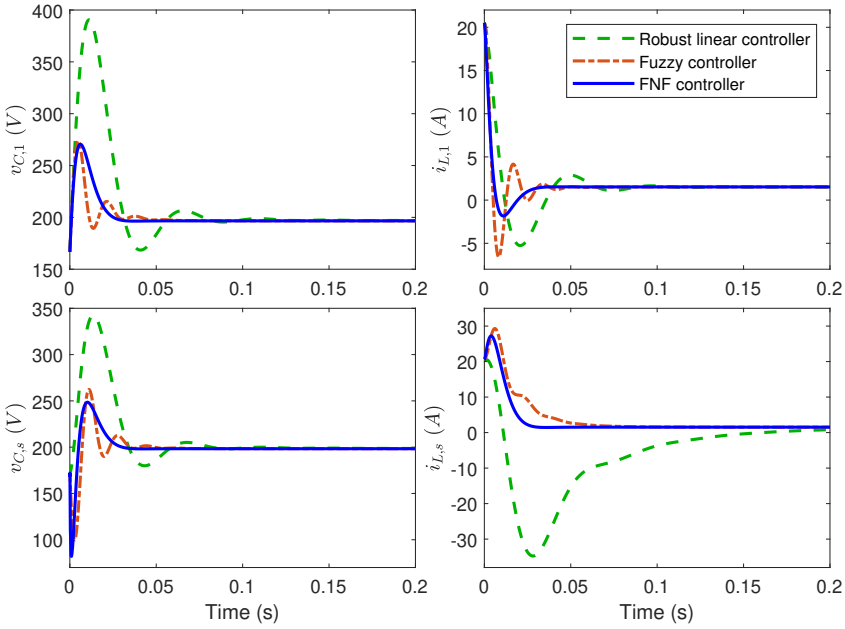

Figure 9: Performances of the robust linear controller [7], fuzzy controller [25] and FNF controller.

Table 5: Settling time and overshoot under different controllers

Methods	Settling time (ms)				Overshoot (%)			
	$v_{C,1}$	$v_{C,s}$	$i_{L,1}$	$i_{L,s}$	$v_{C,1}$	$v_{C,s}$	$i_{L,1}$	$i_{L,s}$
Robust linear controller [7]	66.5	51.4	113	320	98.6	72.7	445	2378
Fuzzy controller [25]	25.6	30.7	57.2	95.3	39.3	49.8	532	1821
FNF controller	**21.0**	**23.2**	**32.2**	**38.0**	**37.6**	**58.7**	**220**	**1685**

As shown in Figure 9 and Table 5, the robust linear controller [7] has the longest settling time and the largest overshoot. The fuzzy controller [25] works better than the robust linear controller [7], since the T-S fuzzy method

is more suitable in handling the CPLs induced nonlinear issue, which confirms Remark 1. The proposed FNF controller performs even better than the fuzzy controller [25], since the uncertainties are considered during the controller design.

5.4. Comparison with the static ETMs [20, 21, 22]

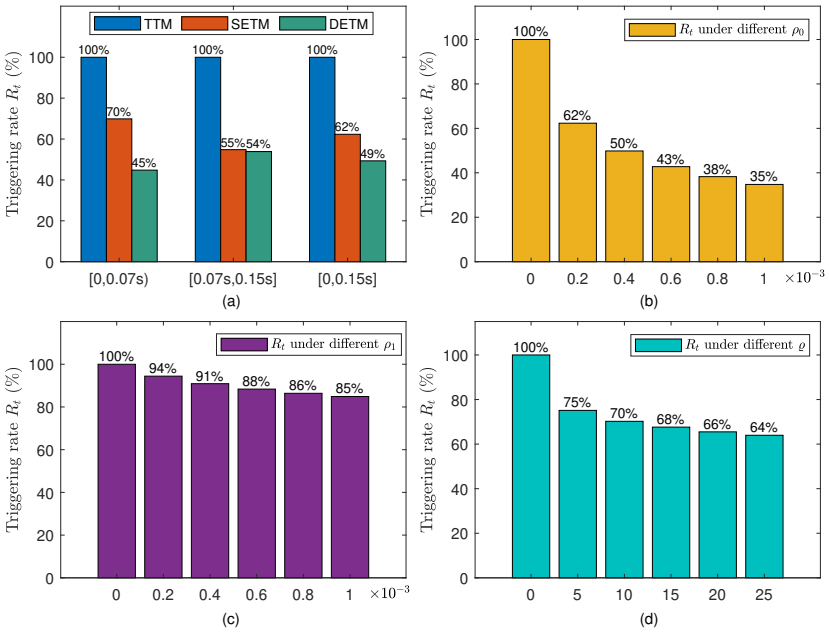

Figure 10: Comparison between the dynamic ETM and the static ETMs [20, 21, 22] (a), and effects of the triggering parameters ρ_0 (b), ρ_1 (c) and ϱ (d).

Figure 10 (a) shows the triggering rates of the dynamic ETM (11) ($\rho_0 = 0.0002, \rho_1 = 0.0008$) and the static ETMs (SETMs) [20, 21, 22] ($\rho_1 = 0$). Compared with the TTM with a transmitting rate 100%, both of the dynamic ETM (11) and static ETMs [20, 21, 22] can reduce the transmitting rate. During the transient response $[0, 0.07s)$, since the large state error $\|\xi(t)\|$ results in a large dynamic threshold $\rho_d(t)$, the dynamic ETM (11) obtains a much lower triggering rate of 45% than 70% for the static ETMs [20, 21, 22]. During the steady response $[0.07s, 0.15s]$, the small $\|\xi(t)\|$ leads to a small dynamic threshold $\rho_d(t)$, and thus the dynamic ETM (11) still achieves a slightly lower triggering rate of 54% than 55% for the static ETMs [20, 21, 22], which confirms Remark 3. During the whole running time $[0, 0.15s]$, due to the addition

of the dynamic triggering threshold $\rho_d(t)$, the dynamic ETM (11) obtains a lower triggering rate of 49% than 62% for the static ETMs [20, 21, 22].

Figure 10 (b), (c) and (d) present the effects of the triggering parameters $(\rho_0, \rho_1, \varrho)$ on the triggering rate R_t of the dynamic ETM (11). Clearly, as the parameter $\rho_0/\rho_1/\varrho$ increases, the triggering rate R_t of the dynamic ETM decreases, which makes it convenient to adjust the triggering rate of the dynamic ETM. Besides, according to the definition (11) of the dynamic ETM and Remark 3, the parameters (ρ_1, ϱ) and ρ_0 play a major role in reducing the triggering rate during the transient response and steady response, respectively.

5.5. Comparison with the DETMs [29, 30, 31, 32]

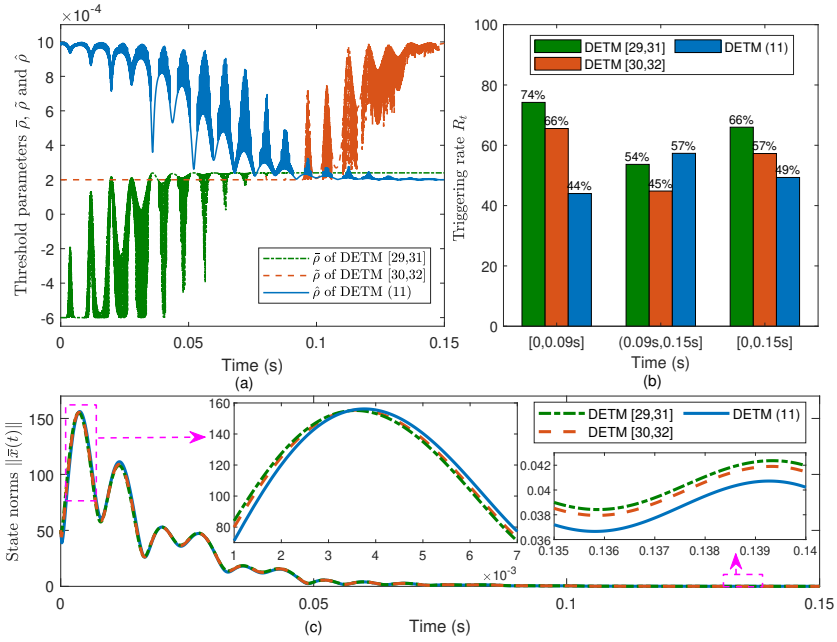

Figure 11: Comparison with the DETMs [29, 31] and the DETMs [30, 32]

Figure 11 (a) shows $\bar{\rho}$ of the DETMs [29, 31] $(\eta = 0.0002, a = 4, \theta = 0.05)$, $\tilde{\rho}$ of the DETMs [30, 32] $(\sigma_1 = 0.0002, \sigma_2 = 0.0008, \varsigma = 0.2)$ and $\hat{\rho}$ of the DETM (11) $(\rho_0 = 0.0002, \rho_1 = 0.0008)$. The triggering rates of these DETMs are presented in Figure 11 (b). During the transient response (i.e, $t \in [0, 0.09s]$), since $\hat{\rho}$ is larger than $\tilde{\rho}$ and $\bar{\rho}$, the DETM (11) obtains the lowest triggering

rate 44%. During the steady-state response (i.e, $t \in (0.09s, 0.15s]$), both of $\tilde{\rho}$ and $\bar{\rho}$ are larger than $\hat{\rho}$, and thus the DETM (11) has the highest triggering rate 57%. As shown in Figure 11 (c), these DETMs generally obtain similar control performances. In detail, as shown in the zoomed graphs, during the transient response, since the DETM (11) has the lowest triggering rate, the system convergence speed is slightly slower. During the steady-state response, due to the usage of the highest triggering rate, the DETM (11) ensures smaller steady-state errors, which implies the tradeoff between control and communication performances. The performances of the DETMs [29, 30, 31, 32] are opposite to that of the DETM (11). These observations confirm Remark 4.

Remark 12. In this section, the main performance evaluation indicators are chosen as follows. For the dynamic ETM, the triggering rate is a critical index, since it implies how much network bandwidth can be saved. For the FDI attacks, the attacking rate is a key indicator, since it describes how frequent the control signals are tampered. For the controllers, the settling time and overshoot of system states are important indexes, since they directly reflect the controllers' performance.

Remark 13. Using the type-1 fuzzy method, this paper designs a SFNF controller for the DC microgrids with known dynamics. For Markov jump systems with unknown dynamics, the work [45] proposes an optimal fuzzy control strategy based on the reinforcement learning. To handle the parameters uncertainties in membership functions, the work [46] presents an interval type-2 fuzzy filter for fault detection. In the future, the methods [45, 46] can be used to analyse the DC microgrids with unknown dynamics and parameter uncertainties.

Remark 14. Considering effects of the dynamic ETM, plant and controller uncertainties, FDI attacks, saturation, network delays and premise mismatching, it is not easy to build the closed-loop system model (18). Besides, nonlinear coupled terms are induced in stability criteria in Theorem 1, which makes it difficult to design controller. Thus, although the used theory is not complicated, the system analysis and synthesis are not easy. Simulation shows that, although the SFNF controller (14) and dynamic ETM (11) are not complicated, they can guarantee satisfied control and communication performances with low computation burden.

Remark 15. Unlike this paper which focuses on the DC microgrids with known dynamics, the work [45] proposes a reinforcement learning based optimal fuzzy control strategy for markov jump systems with unknown dynamics. Unlike this paper which uses type-1 fuzzy method, the work [46] presents an interval type-2 (IT2) fuzzy filter for fault detection, and the work [47] proposes an IT2 based fuzzy fault tolerant control method for stochastic switched systems. Based on IT2 fuzzy neural networks, the work [48] presents a fuzzy sliding mode control method for DC-DC converters. In future, the IT2 fuzzy control and optimal fuzzy control methods can be used to study complex microgrid systems.

6. Conclusion

This paper investigates the fuzzy non-fragile control of DC microgrids affected by the dynamic ETM, FDI attacks, uncertainties, controller saturation, network delays and premise mismatching. First, a discrete-time dynamic ETM is proposed. By adding a dynamic triggering threshold, the dynamic ETM achieves a lower triggering rate than the static ETMs. Since the MIET of the dynamic ETM is lower bounded by the sampling period, Zeno behavior is naturally avoided. Then, using the T-S fuzzy and time-delay modeling methods, a fuzzy time-delay closed-loop system model is established, which facilitates studying the effects of all the affecting factors in a unified framework. Next, using the Lyapunov stability theory, criteria for exponential stability in mean square are obtained, which establish the relationship between system stability and the affecting factors. Further, using the LMI technology, parameters of the SFNF controller and the dynamic ETM can be co-designed. Simulation results confirm the effectiveness of the proposed method. Based on the results of the single-bus DC microgrid studied in this paper, the cooperative control of multi-bus microgrids and AC/DC hybrid microgrids will be studied in the future.

Declaration of competing interest

The authors declare that they have no known competing financial interests or personal relationships that could have appeared to influence the work reported in this paper.

Acknowledgments

This work was supported by National Natural Science Foundation of China under grant 61703146, 62173218; Scientific Project in Henan Province under grant 232102110268, 202102110126; Backbone Teacher in Henan Province under grant 2020GGJS048; International Corporation Project of Shanghai Science and Technology Commission under Grant 21190780300.

References

[1] S. S. Zehra, A. U. Rahman, H. Armghan, I. Ahmad, U. Ammara, Artificial intelligence-based nonlinear control of renewable energies and storage system in a DC microgrid, ISA Transactions 121 (2022) 217 – 231.

[2] M. Cespedes, L. Xing, J. Sun, Constant-power load system stabilization by passive damping, IEEE Transactions on Power Electronics 26 (7) (2011) 1832–1836.

[3] S. Fan, F. Wu, H. Liu, Unified closed-loop control and parameters design of buck-boost current-fed isolated DC-DC converter with constant power load, IEEE Journal of Emerging and Selected Topics in Power Electronics 10 (4) (2022) 4207 – 4217.

[4] Q. Xu, N. Vafamand, L. Chen, T. Dragičević, L. Xie, F. Blaabjerg, Review on advanced control technologies for bidirectional DC/DC converters in DC microgrids, IEEE Journal of Emerging and Selected Topics in Power Electronics 9 (2) (2021) 1205–1221.

[5] S. Hu, D. Yue, C. Dou, X. Xie, Y. Ma, L. Ding, Attack-resilient event-triggered fuzzy interval type-2 filter design for networked nonlinear systems under sporadic denial-of-service jamming attacks, IEEE Transactions on Fuzzy Systems 30 (1) (2022) 190–204.

[6] H. Azmi, A. Yazdizadeh, Robust adaptive fault detection and diagnosis observer design for a class of nonlinear systems with uncertainty and unknown time-varying internal delay, ISA Transactions 131 (2022) 31–42.

[7] L. Herrera, W. Zhang, J. Wang, Stability analysis and controller design of DC microgrids with constant power loads, IEEE Transactions on Smart Grid 8 (2) (2017) 881 – 888.

[8] M. Boukerdja, A. Chouder, L. Hassaine, B. O. Bouamama, W. Issa, K. Louassaa, H_∞ based control of a DC/DC buck converter feeding a constant power load in uncertain DC microgrid system, ISA Transactions 105 (2020) 278 – 295.

[9] N. Vafamand, M. H. Khooban, T. Dragicevic, F. Blaabjerg, J. Boudjadar, Robust non-fragile fuzzy control of uncertain DC microgrids feeding constant power loads, IEEE Transactions on Power Electronics 34 (11) (2019) 11300 – 11308.

[10] C. Peng, F. Li, A survey on recent advances in event-triggered communication and control, Information Sciences 457-458 (2018) 113 – 125.

[11] L. Xing, Q. Xu, F. Guo, Z.-G. Wu, M. Liu, Distributed secondary control for DC microgrid with event-triggered signal transmissions, IEEE Transactions on Sustainable Energy 12 (3) (2021) 1801 – 1810.

[12] H. Zhao, W. Guo, Coordinated control method of multiple hybrid energy storage systems based on distributed event-triggered mechanism, International Journal of Electrical Power and Energy Systems 127 (2021) 106637.

[13] P. Shafiee, Y. Khayat, Y. Batmani, Q. Shafiee, J. M. Guerrero, On the design of event-triggered consensus-based secondary control of DC microgrids, IEEE Transactions on Power Systems 37 (5) (2022) 3834 – 3846.

[14] Z. Cao, J. Zhao, Passivity-based event-triggered control for a class of switched nonlinear systems, ISA Transactions 125 (2022) 50 – 59.

[15] M. Ghiasi, T. Niknam, Z. Wang, M. Mehrandezh, M. Dehghani, N. Ghadimi, A comprehensive review of cyber-attacks and defense mechanisms for improving security in smart grid energy systems: past, present and future, Electric Power Systems Research 215 (2023) 108975.

[16] A. Cecilia, S. Sahoo, T. Dragicevic, R. Costa-Castello, F. Blaabjerg, Detection and mitigation of false data in cooperative DC microgrids with unknown constant power loads, IEEE Transactions on Power Electronics 36 (8) (2021) 9565 – 9577.

[17] A. Cecilia, S. Sahoo, T. Dragicevic, R. Costa-Castello, F. Blaabjerg, On addressing the security and stability issues due to false data injection attacks in DC microgrids - an adaptive observer approach, IEEE Transactions on Power Electronics 37 (3) (2022) 2801 – 2814.

[18] A. Abazari, M. Zadsar, M. Ghafouri, R. Atallah, C. Assi, A data mining/ANFIS and adaptive control for detection and mitigation of attacks on DC MGs, IEEE Transactions on Smart Grid 14 (3) (2023) 2406–2422.

[19] H. Sai, Z. Xu, S. He, E. Zhang, L. Zhu, Adaptive nonsingular fixed-time sliding mode control for uncertain robotic manipulators under actuator saturation, ISA Transactions 123 (2022) 46 – 60.

[20] X.-C. Shangguan, Y. He, C.-K. Zhang, L. Jiang, M. Wu, Load frequency control of time-delayed power system based on event-triggered communication scheme, Applied Energy 308 (2022) 118294.

[21] J. Liu, Y. Wang, L. Zha, X. Xie, E. Tian, An event-triggered approach to security control for networked systems using hybrid attack model, International Journal of Robust and Nonlinear Control 31 (12) (2021) 5796 – 5812.

[22] J. Zhang, H. Zhang, A high-reliability event-triggered secondary control strategy for microgrid considering time-varying delay, IEEE Systems Journal 17 (1) (2023) 617–628.

[23] M. M. Mardani, N. Vafamand, M. H. Khooban, T. Dragievi, F. Blaabjerg, Design of quadratic D-stable fuzzy controller for DC microgrids with multiple CPLs, IEEE Transactions on Industrial Electronics 66 (6) (2019) 4805 – 4812.

[24] D. Marx, S. Pierfederici, B. Nahid-Mobarakeh, B. Davat, Contribution to determination of domain of attraction in power systems: Application to drives with input filter, Houston, TX, United states, 2009.

[25] X. Chen, C. Hu, E. Tian, C. Peng, Event-based fuzzy resilient control of nonlinear DC microgrids under denial-of-service attacks, ISA Transactions 127 (2022) 206 – 215.

[26] C. Peng, T. C. Yang, Event-triggered communication and H_∞ control co-design for networked control systems, Automatica 49 (5) (2013) 1326 – 1332.

[27] D. P. Borgers, W. P. M. H. Heemels, Event-separation properties of event-triggered control systems, IEEE Transactions on Automatic Control 59 (10) (2014) 2644 – 2656.

[28] W. P. M. H. Heemels, J. H. Sandee, P. P. J. V. D. Bosch, Analysis of event-driven controllers for linear systems, International Journal of Control 81 (4) (2008) 571–590.

[29] J. Wang, D. Wang, L. Su, J. H. Park, H. Shen, Dynamic event-triggered H_∞ load frequency control for multi-area power systems subject to hybrid cyber attacks, IEEE Transactions on Systems, Man, and Cybernetics: Systems 52 (12) (2022) 7787 – 7798.

[30] B. Li, S. Hu, Q. Zhong, K. Shi, S. Zhong, Dynamic memory event-triggered proportional-integral-based H_∞ load frequency control for multi-area wind power systems, Applied Mathematics and Computation 453 (2023) 128070.

[31] M. Chen, H. Yan, H. Zhang, Y. Tian, C. Chen, Dynamic event-triggered control of singularity-perturbed dynamic networks and its application, IEEE Transactions on Circuits and Systems II: Express Briefs 69 (7) (2022) 3274 – 3278.

[32] I. Ahmad, X. Ge, Q.-L. Han, Decentralized dynamic event-triggered communication and active suspension control of in-wheel motor driven electric vehicles with dynamic damping, IEEE/CAA Journal of Automatica Sinica 8 (5) (2021) 971 – 986.

[33] D. Yue, E. Tian, Q. L. Han, A delay system method for designing event-triggered controllers of networked control systems, IEEE Transactions on Automatic Control 58 (2) (2013) 475 – 481.

[34] L. Sun, Y. Wang, G. Feng, Control design for a class of affine nonlinear descriptor systems with actuator saturation, IEEE Transactions on Automatic Control 60 (8) (2015) 2195 – 2200.

[35] Y. Wang, Y. Zheng, X. Xie, J. Yang, An improved reduction method based networked control against false data injection attacks and stochastic input delay, Applied Mathematics and Computation 385 (2020) 125421.

[36] L. Zou, Z. Wang, Q.-L. Han, D. Zhou, Ultimate boundedness control for networked systems with try-once-discard protocol and uniform quantization effects, IEEE Transactions on Automatic Control 62 (12) (2017) 6582–6588.

[37] Z. Ye, W.-A. Zhang, D. Zhang, H. Ni, On design of robust sliding mode observer for nonlinear networked time-delay systems with communication constraints, ISA Transactions 124 (2022) 260 – 270.

[38] P. Park, J. W. Ko, C. Jeong, Reciprocally convex approach to stability of systems with time-varying delays, Automatica 47 (1) (2011) 235 – 238.

[39] Z. Gu, X. Sun, H.-K. Lam, D. Yue, X. Xie, Event-based secure control of T-S fuzzy-based 5-DOF active semivehicle suspension systems subject to DoS attacks, IEEE Transactions on Fuzzy Systems 30 (6) (2022) 2032–2043.

[40] A. Armghan, M. K. Azeem, H. Armghan, M. Yang, F. Alenezi, M. Hassan, Dynamical operation based robust nonlinear control of DC microgrid considering renewable energy integration, Energies 14 (13) (2021) 3988.

[41] Q.-Q. Zhang, R.-J. Wai, Robust power sharing and voltage stabilization control structure via sliding-mode technique in islanded micro-grid, Energies 14 (4) (2021) 883.

[42] S. Hu, D. Yue, Event-triggered control design of linear networked systems with quantizations, ISA Transactions 51 (1) (2012) 153–162.

[43] Q. Zhang, X. Yin, S. Hu, A two-event-generator scheme for event-triggered control of uncertain NCSs under deception attacks, Information Sciences 584 (2022) 148–169.

[44] W. Wang, R. Postoyan, D. Nesic, W. Heemels, Periodic event-triggered control for nonlinear networked control systems, IEEE Transactions on Automatic Control 65 (2) (2020) 620 – 635.

[45] H. Fang, Y. Tu, H. Wang, S. He, F. Liu, Z. Ding, S. S. Cheng, Fuzzy-based adaptive optimization of unknown discrete-time nonlinear markov jump systems with off-policy reinforcement learning, IEEE Transactions on Fuzzy Systems 30 (12) (2022) 5276 – 5290.

[46] X. Zhang, H. Wang, V. Stojanovic, P. Cheng, S. He, X. Luan, F. Liu, Asynchronous fault detection for interval type-2 fuzzy nonhomogeneous higher level markov jump systems with uncertain transition probabilities, IEEE Transactions on Fuzzy Systems 30 (7) (2022) 2487 – 2499.

[47] J. Sun, H. Zhang, Y. Wang, S. Sun, Fault-tolerant control for stochastic switched IT2 fuzzy uncertain time-delayed nonlinear systems, IEEE Transactions on Cybernetics 52 (2) (2022) 1335–1346.

[48] J. Wang, W. Luo, J. Liu, L. Wu, Adaptive type-2 FNN-based dynamic sliding mode control of DC-DC boost converters, IEEE Transactions on Systems, Man, and Cybernetics: Systems 51 (4) (2021) 2246 – 2257.